NASA TECHNICAL NOTE

NASA TN D-5798

c. 1

NASA TN D-5798

FURTHER EXPERIMENTAL RESULTS ON THE INFLUENCE OF THE TURBULENT BOUNDARY LAYER ON PANEL FLUTTER

by Peter A. Gaspers, Jr., Lado Muhlstein, Jr., and Daniel N. Petroff

Ames Research Center
Moffett Field, Calif. 94035

NATIONAL AERONAUTICS AND SPACE ADMINISTRATION • WASHINGTON, D. C. • MAY 1970

1. Report No. NASA TN D-5798	2. Government Accession No.	3. Recipient's Catalog No.
4. Title and Subtitle FURTHER EXPERIMENTAL RESULTS ON THE INFLUENCE OF THE TURBULENT BOUNDARY LAYER ON PANEL FLUTTER		5. Report Date May 1970 6. Performing Organization Code
7. Author(s) Peter A. Gaspers, Jr., Lado Muhlstein, Jr., and Daniel N. Petroff		8. Performing Organization Report No. A-3454
9. Performing Organization Name and Address NASA Ames Research Center Moffett Field, Calif. 94035		10. Work Unit No. 126-14-02-01-00-21 11. Contract or Grant No.
12. Sponsoring Agency Name and Address National Aeronautics and Space Administration Washington, D. C. 20546		13. Type of Report and Period Covered Technical Note 14. Sponsoring Agency Code

15. Supplementary Notes

16. Abstract

Flutter boundaries were obtained for a flat rectangular panel for ratios of boundary-layer thickness to panel length of 0.036 to 0.128 at Mach numbers of 1.2 to 1.4. The panel was isotropic and unstressed with a length-to-width ratio of 0.5 and the edges were rotationally restrained to approximate a clamped condition. The results show that the turbulent boundary layer has a large stabilizing influence. The effect is most pronounced at a Mach number of 1.2 and decreases rapidly as the Mach number increases. The experimental results, extrapolated to zero boundary-layer thickness, are compared with the available theoretical predictions. A theoretical analysis of the vibration of plates with variable rotational edge restraint is given and, within its framework, the edge restraint parameters for the experimental panels are determined.

17. Key Words Suggested by Authors Panel flutter, turbulent boundary Layer, low supersonic Rotational edge restraint	18. Distribution Statement Unclassified - Unlimited

19. Security Classif. (of this report) Unclassified	20. Security Classif. (of this page) Unclassified	21. No. of Pages 45	22. Price* $3.00

*For sale by the Clearinghouse for Federal Scientific and Technical Information
Springfield, Virginia 22151

SYMBOLS

a panel dimension in streamwise direction, in.

a_{ij} see equations (A11)

b panel dimension in cross-stream direction, in.

b_{ij} see equations (A11)

C speed of sound, ft/sec

C_p pressure coefficient, $\frac{p - p_\infty}{q_\infty}$

D flexural rigidity of plate, $\frac{Eh^3}{12(1 - \nu^2)}$

E modulus of elasticity, lb/in.^{2}

f frequency, Hz

H wall displacement, in.

h panel thickness, in.

K supersonic reduced frequency, $\frac{kM}{\beta^2}$

k stiffness parameter, $\sqrt{\frac{\tau^2 E}{C_\infty{}^2 \rho_s (1 - \nu^2)}}$ (measured E, assuming clamped edges, see p. 8)

k^* stiffness parameter using handbook value of E

k_1 stiffness parameter, $\frac{\omega_1 a}{V_\infty} = \left(\frac{\lambda_1}{12M^2}\right)^{1/2} k$

k reduced frequency, $\frac{\omega a}{V_\infty}$

L differential operator (see eq. (A3))

M Mach number

m mass per unit area of panel, slugs/ft^2

p static pressure, lb/ft^2

p_t total pressure, lb/ft^2

Δp differential pressure, $p_c - p_\infty$, lb/ft^2

q dynamic pressure, $\frac{\rho_\infty V_\infty^2}{2}$, lb/ft^2

$q_{\xi 0}$ dimensionless rotational restraint parameter, $\frac{a\theta_{x_0}}{D}$

T static temperature, °R

T_t total temperature, °R

ΔT panel-frame differential temperature, $(T_{panel} - T_{frame})$, °F

t time, sec

U spatial part of displacement (see p. 12)

V velocity, ft/sec

W dimensionless panel displacement (see p. 11)

W^* peak panel displacement at transducer location, in.

w transverse panel displacement, in.

x,y rectangular coordinates

α coefficient of thermal expansion, in./in./°F

α_ξ, β_ξ see equations (A13)

β $\sqrt{M^2 - 1}$

δ boundary-layer geometric thickness, distance from wall to point where $\frac{V}{V_\infty} = 0.98$, in.

δ^* boundary-layer displacement thickness, $\int_0^\delta \left(1 - \frac{\rho V}{\rho_\infty V_\infty}\right) dy$, in.

$\delta_{M=1.0}$ distance from wall to point in boundary layer where $M = 1.0$, in.

η dimensionless coordinate, $\frac{y}{b}$

θ boundary-layer momentum thickness, $\int_0^\delta \frac{\rho V}{\rho_\infty V_\infty}\left(1 - \frac{V}{V_\infty}\right) dy$, in.

θ_x, θ_y see page 4

θ_{x0} rotational spring constant per unit length along x = 0 edge of plate, lb-ft/ft

λ dynamic pressure parameter, $\frac{2qa^3}{\beta D}$

λ_n nth eigenvalue of plate

μ mass ratio parameter, $\frac{\rho_\infty a}{\rho_s h}$

μ_c cavity mass ratio parameter, $\frac{\rho_c a}{\rho_s h}$

ν Poisson's ratio

ξ dimensionless coordinate, $\frac{x}{a}$

ρ density, slugs/ft^3

τ panel thickness-to-length ratio, $\frac{h}{a}$; also dimensionless time

ϕ_n, Ψ_m see equations (A13)

ω circular frequency, rad/sec

ω_n nth natural frequency of plate, rad/sec

Subscripts

c cavity

F flutter

s structure (panel)

∞ free stream

FURTHER EXPERIMENTAL RESULTS ON THE INFLUENCE OF THE TURBULENT BOUNDARY LAYER ON PANEL FLUTTER

Peter A. Gaspers, Jr., Lado Muhlstein, Jr.,
and Daniel N. Petroff

Ames Research Center

SUMMARY

Flutter boundaries were obtained for a flat rectangular panel for ratios of boundary-layer thickness to panel length of 0.036 to 0.128 at Mach numbers of 1.2 to 1.4. The panel was isotropic and unstressed with a length-to-width ratio of 0.5 and the edges were rotationally restrained to approximate a clamped condition. The results show that the turbulent boundary layer has a large stabilizing influence. The effect is most pronounced at a Mach number of 1.2 and decreases rapidly as the Mach number increases. The experimental results, extrapolated to zero boundary-layer thickness, are compared with the available theoretical predictions. A theoretical analysis of the vibration of plates with variable rotational edge restraint is given and, within its framework, the edge restraint parameters for the experimental panels are determined.

INTRODUCTION

Experimental data in a previous report (ref. 1) showed that the turbulent boundary layer has a large stabilizing influence on panel flutter at low supersonic Mach numbers. In that study the Mach numbers ranged from 1.05 to 1.4, the stiffness parameter was about 0.072, and the mass ratio parameter ranged from 0.06 to 0.11. In the present study additional experimental results have been obtained for Mach numbers from 1.2 to 1.4 but for a stiffness parameter of about 0.025 and mass ratios of 0.009 to 0.017. The panel made of Invar was flat, rectangular (length-to-width ratio 0.5), and unstressed with rotationally restrained, approximately clamped, edges. Extensive precautions, discussed in detail in reference 1, were taken to eliminate as many as possible of the usual sources of experimental inaccuracy. The results from reference 1 and from the present investigation, including extrapolations to zero boundary-layer thickness, are compared with theoretical predictions based on three-dimensional unsteady potential flow. The present results support the findings of reference 1 and show that the influence of the boundary layer can account for a substantial portion of the disagreement between theoretical and experimental panel flutter results in the low supersonic Mach number range (refs. 1-4).

APPARATUS

Panel Configuration

Dimensions and mounting details of the panel and frame used in this experiment are shown in figure 1. The 9.00-inch by 18.00-inch by 0.0192-inch-thick panel was made from Invar, an iron-nickel alloy (64-percent iron, 36-percent nickel) with a very low coefficient of thermal expansion. The panel was attached to an Invar frame, 11.00 inch by 20.00 inch by 0.340 inch thick, with an adhesive (Eastman 910).

Closely spaced roundhead screws were threaded into the panel sheet from the cavity side (air stream side smooth) to provide additional clamping action and to prevent loss of the panel in case of bond failure during flutter. Comparison of panel natural frequencies before and after the flutter test disclosed no deterioration of the adhesive bond.

The panel frame was attached to the test fixture by one high-stiffness and two low-stiffness flexures as shown in figure 1. This three-point mounting was designed to minimize the introduction of external stresses into the panel frame.

Wind Tunnel

The experiments were conducted in the Ames 2- by 2-Foot Transonic Wind Tunnel, which is of the continuous flow type with porous test section walls surrounded by a plenum chamber (see ref. 5). Mach number is continuously variable from 0.60 to 1.40 and dynamic pressure is continuously variable from 200 to 1500 psf.

Variable Boundary-Layer Test Fixture

The fixture for varying the boundary-layer thickness consisted of a splitter plate with a sharp leading edge installed in one side wall of the wind tunnel. This splitter plate could be positioned by remote control to be flush with the wall or to project up to 1.0 inch into the airstream. Dimensions of the test fixture are shown in figure 2. When the splitter plate was flush with the tunnel wall, the boundary-layer thickness in the test region was maximum. When the splitter plate was moved into the airstream, a portion of the tunnel-wall boundary layer was directed into the plenum chamber surrounding the test section and a thinner boundary layer was established on the splitter plate. The boundary-layer thickness in the panel test region is variable by this means between the approximate limits of 0.25 and 1.00 inch. Boundary-layer thickness was measured by four retractable boundary-layer total-pressure probes located as shown in figure 2. Figures 3 and 4 are front and rear views and show tunnel installation of the variable boundary-layer test fixture.

Other Equipment

The panel was backed by a sealed rectangular cavity (identical to that used in ref. 1) with the same dimensions as the panel and with an effective depth of 7.5 inches (where effective depth is defined as the actual cavity volume minus volume occupied by instrumentation all divided by panel area). The panel frame was sealed to the cavity with adhesive plastic tape to minimize the possibility of introducing stresses into the panel frame.

The differential pressure between the cavity and free stream was controlled manually to within ±0.25 psf by a system similar to that described in reference 2.

Panel Natural Frequencies, Material Properties, and Boundary Conditions

In order to calculate the natural frequencies of a plate accurately, the plate dimensions, elastic constants, density, and boundary conditions must be known accurately. The plate dimensions and density can be measured to almost an arbitrary degree of accuracy and so present no problem. Determining the elastic constants and boundary conditions, however, presents difficulties since the two effects are not easily separated. One method (ref. 6) of determining the elastic constants of thin isotropic plates depends on the fact that the normalized frequency spectrum of a plate with free edges is a function of Poisson's ratio. Therefore, for the free plate the experimentally obtained ratio of any two natural frequencies together with the value of any natural frequency determines Poisson's ratio and Young's modulus. The free circular plate is most convenient for this purpose because its eigenvalues can be calculated exactly.

This method was used here to redetermine the elastic constants of the magnesium alloy sheet material used in reference 1 and the results are shown in table 1. The resulting Young's modulus of 6.2×10^6 psi lies between our previous measured value of 5.6×10^6 psi and the handbook value of 6.5×10^6 psi. The value of Poisson's ratio coincides with the handbook value. When the same method was applied to the Invar sheet material, an unacceptably large amount of data scatter was obtained and so, for that case, the handbook values are used. The failure of this method for the Invar sheet material may be due to residual stresses or small variations in thickness or flatness. The eigenvalues of a free plate depend rather weakly on Poisson's ratio and any variations between the experimental specimen and the theoretical model can be expected to cause difficulty.

The boundary conditions of the magnesium panel and of the Invar panel were determined within the framework of an analytical model that prescribed zero transverse edge displacement but arbitrary rotational edge restraint. A theoretical analysis of this model together with some typical numerical results is presented in the appendix. The same theoretical model is analyzed in reference 7 by a different method. It was assumed that $q_{\xi 0} = q_{\xi 1} = q_{\xi}$ and $q_{\eta 0} = q_{\eta 1} = q_{\eta}$ (equal rotational restraints on opposite panel edges); then q_{ξ} and q_{η} were determined to give a least squares fit to the experimental

natural frequencies. The resulting values of q_ξ and q_η (see table 1) show that the magnesium panel was considerably closer to the clamped condition than the Invar panel. The lower values of the restraint parameter for the Invar panel are probably associated with the adhesive bonded joint between panel and frame (the magnesium panel of ref. 1 was an integral part of the frame), but the detailed mechanism of declamping is not clear. The ratio of q_η to q_ξ for both panels is much larger than the theoretical value of 2 which results if the dimensional rotational spring constants θ_x and θ_y on all four sides are equal. This may be due to the variation of θ_x and θ_y along the edge caused by the torsional and bending stiffness of the frame. It should be noted, however, that as both q_ξ and q_η become large, the panel approaches the clamped condition and the ratio of q_η to q_ξ becomes less significant.

The values of q_ξ and q_η given in table 1 result in a root-mean-square error between theoretical and experimental natural frequencies (the first 5) of 1.3 percent for the magnesium panel and 2.4 percent for the Invar panel. If clamped edges are assumed the RMS errors become 3.6 percent for the magnesium panel and 11.9 percent for the Invar panel.

Thermal Effects

As discussed in some detail in reference 1, a relatively small temperature difference between the panel and frame can have a large effect on the natural frequencies and consequently on the flutter boundary of thin panels. To prevent excessive temperature sensitivity of the low stiffness panel desired for this test, it was constructed of Invar which has a coefficient of thermal expansion approximately 1/20th that of aluminum or magnesium.

The theoretical temperature differential (assuming a clamped panel) between the panel and frame that would buckle this panel is 17.5° F. An experiment described in reference 1 was unable to produce buckling and the change in natural frequency observed was only a fraction of a hertz per °F. The maximum temperature differential between panel and frame was limited to 0.5° F during acquisition of flutter data. Therefore, the influence of temperature differential can be assumed negligible.

INSTRUMENTATION

The instruments used and measurements made during this test are identical to those reported in reference 1. The panel displacement was measured with a noncontacting capacitance-type transducer located as shown in figure 2. The surface static pressures and the total pressures from the boundary-layer probes were measured with conventional strain-gage differential-pressure transducers connected to the orifices by short lengths of tubing and referenced to free-stream static pressure. Panel and frame temperatures were measured with iron-constantan thermocouples in the center of the panel and at two points on the frame. The thermocouple in the center of the panel was constructed of wire 0.005 inch in diameter and was the only object contacting the

panel. Steady quantities such as temperatures and pressures were recorded digitally. Unsteady or slowly varing quantities such as fluctuating static pressure, panel response, and pressure differential between the cavity and free stream were recorded by a frequency modulated magnetic tape recorder with a flat frequency response (±0.5 dB) from dc to 1250 Hz.

TEST PROCEDURE

Flow Conditions in Panel Test Region

The flow conditions in the panel test region are an important consideration in panel flutter testing, as discussed in reference 1. Both the surface static-pressure distribution and the fluctuating pressure were measured. The maximum variation of surface static-pressure coefficient (C_p) is ±0.02, with most variations being less than ±0.01. The power spectra of the fluctuating pressures indicate that there are no dominant frequencies in the range of interest for this investigation. Plots of typical static-pressure distributions, fluctuating pressure coefficients, power spectra of the fluctuating pressures, and boundary-layer velocity profiles for various splitter plate displacements are presented in reference 1.

Determination of the Flutter Boundary

The many problems involved in accurately defining an experimental flutter boundary are discussed in detail in reference 1. In the present study, the flutter boundary is determined in the same manner as in reference 1, namely, which is as follows: At dynamic pressures well below that for flutter, the panel response to pressure disturbances from the turbulent boundary layer increases approximately linearly with dynamic pressure, as indicated in figure 5. In this figure, panel amplitude in the mode which becomes the flutter mode is shown as a function of dynamic pressure. This "subflutter response" is used as a reference level to define the flutter point systematically. The straight lines labeled 2x, 3x, etc., in figure 5 are multiples of the subflutter response. Their intersections with the amplitude response curve define values of dynamic pressure necessary to produce panel amplitudes which are these multiples of the subflutter response. Figure 6 shows dynamic pressure as a function of the multiples of the subflutter response for the same conditions as shown in figure 5. As the multiple increases, the difference in dynamic pressure between successive multiples decreases; that is, the dynamic pressure appears to be converging to a limit. Furthermore it appears that the 6x multiple results in a dynamic pressure very close to this limiting dynamic pressure and is therefore arbitrarily defined herein as the flutter point.

The following test procedure was adhered to throughout the program. Mach number and splitter plate position were held constant while dynamic pressure was increased in small increments beginning at a value well below the flutter boundary. After each increase in dynamic pressure, the panel-frame temperature differential was allowed to stabilize to ±0.5° F to minimize thermal stress effects. The indicated differential pressure between the cavity and free stream was then varied slowly from -50 to +50 psf while the panel

response was recorded. It is assumed that the maximum response so measured corresponds to zero average differential pressure across the panel. Next the indicated differential pressure was set to the value at which maximum response occurred. This response was recorded so that amplitude spectra could be obtained with all test conditions fixed. The above procedure was repeated for each increase in dynamic pressure until the maximum response was a large-amplitude, essentially sinusoidal motion indicating that the flutter boundary had been penetrated. Boundary-layer velocity profiles were obtained at dynamic pressures near the flutter boundary. The forward probe was retracted while data were being recorded from the rear probes, and all probes were retracted when boundary-layer data were not being recorded.

The maximum response amplitude of the panel mode which becomes the flutter mode was determined from plots of response amplitude versus differential pressure for each dynamic pressure with the special data reduction system described in reference 1.

RESULTS AND DISCUSSION

Influence of the Turbulent Boundary Layer on Flutter Dynamic Pressure

The dynamic pressures for various multiples of subflutter response for a series of boundary-layer thicknesses are shown in figure 7 for Mach numbers of 1.20, 1.30, and 1.40. The geometric boundary-layer thickness used is the thickness in the center of the panel, estimated by assuming linear growth between the upstream and downstream probes. The curve for 6x subflutter response is considered the flutter boundary. The flutter dynamic pressure in figure 7 is approximately a linear function of the geometric boundary-layer thickness, thus allowing reasonable extrapolation to zero boundary-layer thickness.

In figure 8 the flutter dynamic pressure normalized by the extrapolated flutter dynamic pressure for zero boundary-layer thickness at that Mach number ($q/q_{\delta=0}$) is plotted as a function of the ratio of boundary-layer thickness to panel length (δ/a). The slopes of the curves in figure 8 $d(q/q_{\delta=0})/d(\delta/a)$ are plotted as a function of Mach number in figure 9, which shows the strong dependence of boundary-layer effects on Mach number. The maximum effect occurs below $M = 1.20$, the minimum Mach number in this experiment, and is similar to the result reported in reference 1.

Influence of the Turbulent Boundary Layer on Flutter Frequency

The flutter frequency normalized by the flutter frequency for zero boundary-layer thickness ($f/f_{\delta=0}$), obtained by linear extrapolation in the manner of reference 1, is plotted versus the normalized boundary-layer thickness in figure 10. Note that an increase in boundary-layer thickness causes a decrease in flutter frequency.

The slopes of the curves in figure 10, $d(f/f_{\delta=0})/d(\delta/a)$, are presented in figure 11 as a function of Mach number and indicate that the minimum effect of boundary-layer thickness on flutter frequency for this panel occurs near $M = 1.30$.

The results shown in figure 10 are replotted in figure 12 where the reduced frequency of flutter is presented as a function of Mach number for various normalized boundary-layer thicknesses.

Generalized Panel Flutter Boundaries

A natural set of dimensionless parameters for the flutter of flat isotropic panels exposed to linearized three-dimensional unsteady potential flow (ref. 8) is the mass ratio parameter, $\mu = \rho_\infty a/\rho_s h$, the stiffness parameter, $k = \sqrt{\tau^2 E/C_\infty^2 \rho_s (1 - \nu^2)}$, the panel length-to-width ratio, a/b, the Mach number M, and the reduced frequency k. Flutter boundaries, along which the reduced frequency varies, may be plotted in the k-μ plane for each combination of Mach number and length-to-width ratio. Various authors have replaced k and μ with other sets of dimensionless parameters (see refs. 2, 9, 10) but all of these alternate sets depend on Mach number, length-to-width ratio, or panel edge conditions and so, as pointed out in reference 8, plots for different Mach numbers, etc., cannot be directly compared. For this reason all flutter boundaries presented herein are plotted in the k-μ plane. If boundary-layer effects are to be considered, the ratio of boundary-layer thickness to panel length, δ/a, and the boundary-layer profile must also be considered. In figure 13, the flutter mass ratio parameter μ is plotted as a function of boundary-layer thickness to panel length ratio δ/a, for the three test Mach numbers. Since these data fall approximately on a straight line, they can reasonably be extrapolated to zero boundary-layer thickness ($\delta/a = 0$) to give a value of μ for comparison with results predicted by potential flow theory.

Comparison With Theoretical Predictions

For the panel length-to-width ratio (a/b) and Mach number range of this test, valid panel flutter predictions can be obtained only by three-dimensional unsteady aerodynamic theory. Theoretical results based on such theory for clamped rectangular panels for the length-to-width ratio and Mach number range of interest are presented in references 2 and 10. These results are used for comparison with the experimental data presented in this report and in reference 1.

In reference 2, a four-mode analysis was performed for a clamped rectangular panel with $a/b = 0.46$. Results are presented for $M = 1.10$, 1.20, 1.30, and $\sqrt{2}$ and structural damping coefficients of 0 and 0.05 in the dynamic pressure parameter-density ratio (λ,μ) plane where the relation between λ, k, and μ is given by

$$\lambda = 12M^2\mu/\beta k^2$$

It should be noted that the adequacy of the four-mode analysis was based on convergence studies using quasi-steady aerodynamics. No convergence studies were performed using three-dimensional unsteady aerodynamics. Although these results are for $a/b = 0.46$, they are expected to differ very little from those for $a/b = 0.5$ and thus are used for comparison without correction. In another approximation in reference 2 the off-diagonal elements of the stiffness matrix are neglected, but in reference 11 it is shown that for length-to-width ratios in the vicinity of 0.5, the effect on the flutter boundary is negligible. For use in this comparison, the λ,μ plots of reference 2 were converted to the k,μ plane. A theoretical boundary for $M = 1.40$ was obtained by plotting μ versus M for various values of k and obtaining the desired μ,k plot by interpolation. Since $M = 1.40$ is not significantly different from $M = \sqrt{2}$, the errors resulting from interpolation are small.

Reference 10 presents flutter boundaries for clamped panels of $a/b = 0.5$ for $M = 1.30$ only. As in reference 2, the off-diagonal elements of the stiffness matrix were neglected. The parameters employed are $\mu_1 = 1/\mu$, where μ is the usual mass ratio parameter (however, $1/\mu_1$ is plotted), and a stiffness parameter

$$k_1 = \frac{\omega_1 a}{V_\infty} = \left(\frac{\lambda_1}{12M^2}\right)^{1/2} k$$

where ω_1 and λ_1 are the lowest natural frequency and eigenvalue, respectively, of the plate. Results of a six-mode analysis are presented for coefficients of structural damping of 0 and 0.01 in the $k_1 - 1/\mu_1$ plane. These results have been converted to the k-μ plane for use herein. The value of $\lambda_1 = 604.05835$ used in the conversions was computed by Galerkin's method using 14 clamped beam modes in both the chordwise and spanwise directions.

In the following comparisons of the experimental results from reference 1 and the present study with the theoretical predictions of references 2 and 10, the Young's modulus used in the stiffness parameter k would result in a first-mode natural frequency for a clamped panel that matches the experimentally determined first natural frequency. Since the theoretical results are for perfectly clamped panels, this choice of E compensates, at least partly, for the less than clamped edge conditions of the experimental panels.

In addition, the stiffness parameter k^*, based on the handbook value of E, is included in table 2 where the various panel flutter parameters, boundary-layer thicknesses, frequencies, and other pertinent quantities are tabulated.

In figure 14(a) the experimental data for $M = 1.3$ in the k-μ plane from reference 1 and the present study are compared with theoretical stability boundaries from references 2 and 10. The stability boundaries from reference 10 are more accurate than those of reference 2 since a six-mode analysis was used in the former case whereas four modes were used in the latter. Theory predicts the existence of several stability boundaries - that giving the largest value of k, for a given μ, being the critical or flutter boundary.

For μ corresponding to the experimental results, the theoretical flutter boundary is that labeled mode 2 which is predominately composed of the second natural, in vacuo, mode. However, the experimental points corresponding to zero boundary-layer thickness for both sets of experimental data fall between the reference 10 mode 1 boundaries for $g = 0$ and 0.01. The mode 1 boundary is predominately composed of the first natural, in vacuo, mode but contains a significant amount of the second natural mode and so it is sometimes called a coupled mode instability. The mode 2 boundary is associated with a very weak instability that completely disappears for a value of g of about 0.02 (ref. 2) and was not observed in the present study or in reference 1. The values of g for the experimental cases were not measured, but, because of the method of panel fabrication, are expected to be in the neighborhood of 0.01 or less. In addition, we note from qualitative observations that the damping of the Invar panel of the present study is considerably less than that of the magnesium panel of reference 1. This is to be expected from thermoelastic considerations (ref. 12) since the thermal expansion coefficient of Invar is very low.

The agreement between experimental and theoretical reduced frequencies for the mode 1 boundary is considered to be only fair. Since the theoretical reduced frequencies associated with the mode 2 boundary are much higher, it is clear that the observed flutter is first mode.

In figure 14(b) the experimental data from reference 1 at $M = 1.1$ is compared to the first-mode theoretical k-μ boundaries from reference 2. As at $M = 1.3$, the agreement between theory and experiment improves as the boundary-layer thickness approaches zero. However, the difference between theoretical and experimental k-μ points for zero boundary-layer thickness is considerably larger than at $M = 1.3$. On the other hand, the experimental and theoretical reduced frequencies are in good agreement.

In figure 14(c) the experimental data from reference 1 and the present study, for $M = 1.2$, are compared with the first-mode theoretical boundary from reference 2. The effect of the boundary layer is very similar to that at $M = 1.1$ and 1.3.

In figure 14(d) the experimental data at $M = 1.4$ are compared with the theoretical boundaries from reference 2. However, in contrast to the lower Mach numbers, as the boundary-layer thickness decreases, the difference between theory and experiment increases for both sets of experimental data. This behavior is difficult to explain since both the boundary layer and structural damping have less effect at $M = 1.4$ than at lower Mach numbers. On the other hand, except at $M = 1.3$, the agreement between theory and experiment for zero boundary-layer thickness is better at $M = 1.4$ than at the lower Mach numbers.

It is interesting to note that the disagreement between theory and experiment is similar for both panels at all Mach numbers, indicating that the disagreement results from some systematic inaccuracy or omission in either theory or experiment rather than random errors in the experimental results. It is possible that a combination of errors, usually considered small individually, such as unconverged solutions, neglect of cavity, omission of off-diagonal terms in stiffness matrix and imprecise matching of boundary

conditions could, taken together, cause an appreciable error in some of the theoretical predictions. It should also be remembered that we have used an arbitrary, though systematic, definition of the flutter boundary and this could cause an error, depending on the strength of the instability.

Finally, it should be noted that Dowell (ref. 13) previously compared the experimental results of reference 1 with the theory from reference 2 and concluded that experimental data from reference 1 for zero boundary-layer thickness agree well with the theory. His conclusion is somewhat stronger than those made herein and it bears repeating that detailed comparisons at these Mach numbers depend strongly on the structural damping.

CONCLUSIONS

For the configuration tested the following conclusions can be noted.

1. The turbulent boundary layer has a large stabilizing influence on the flutter of flat isotropic panels at low supersonic Mach numbers.

2. The effect of the turbulent boundary layer on flutter dynamic pressure decreases rapidly with increasing Mach number above $M = 1.20$ for the configuration tested.

3. The agreement between the experimental results and theoretical predictions based on unsteady, three-dimensional, potential flow is considerably improved when the experimental results are extrapolated to zero boundary-layer thickness except at $M = 1.4$ where the effect of the boundary layer is much smaller than at the lower Mach numbers.

4. The experimental results indicate that flutter occurs as a predominantly first-mode instability rather than the predominantly second-mode instability predicted by theory.

Ames Research Center
National Aeronautics and Space Administration
Moffett Field, Calif., 94035, Jan. 15, 1970

APPENDIX A

NATURAL FREQUENCIES OF RECTANGULAR PLATES WITH ROTATIONALLY RESTRAINED EDGES

The differential equation and boundary conditions for a rectangular isotropic plate with arbitrary rotational edge restraint and zero edge translation are as follows:

$$D(w_{xxxx} + 2w_{xxyy} + w_{yyyy}) + mw_{tt} = 0 \tag{A1}$$

$$\left.\begin{aligned} Dw_{xx} - \theta_{x0}w_x &= 0 , \quad w = 0 \quad \text{on} \quad x = 0 \\ Dw_{xx} + \theta_{xa}w_x &= 0 , \quad w = 0 \quad \text{on} \quad x = a \\ Dw_{yy} - \theta_{y0}w_y &= 0 , \quad w = 0 \quad \text{on} \quad y = 0 \\ Dw_{yy} + \theta_{yb}w_y &= 0 , \quad w = 0 \quad \text{on} \quad y = b \end{aligned}\right\} \tag{A2}$$

where θ_{x0}, etc., are the rotational spring constants per unit length along the edges of the plate and the subscripts on w indicate partial differentiation with respect to the subscript.

Making the transformation:

$$x = a\xi \qquad y = b\eta \qquad w = aW \qquad t = t_o\tau$$

we obtain the following dimensionless form of the equations:

$$W_{\xi\xi\xi\xi} + 2\frac{a^2}{b^2}W_{\xi\xi\eta\eta} + \frac{a^4}{b^4}W_{\eta\eta\eta\eta} + W_{\tau\tau} = LW + W_{\tau\tau} = 0 \tag{A3}$$

$$\left.\begin{aligned} W_{\xi\xi} - q_{\xi 0}W_{\xi} &= 0 , \quad W = 0 \quad \text{on} \quad \xi = 0 \\ W_{\xi\xi} + q_{\xi 1}W_{\xi} &= 0 , \quad W = 0 \quad \text{on} \quad \xi = 1 \\ W_{\eta\eta} - q_{\eta 0}W_{\eta} &= 0 , \quad W = 0 \quad \text{on} \quad \eta = 0 \\ W_{\eta\eta} + q_{\eta 1}W_{\eta} &= 0 , \quad W = 0 \quad \text{on} \quad \eta = 1 \end{aligned}\right\} \tag{A4}$$

where

$$q_{\xi 0} = \frac{a\theta_{x0}}{D} \qquad q_{\xi 1} = \frac{a\theta_{xa}}{D} \qquad q_{\eta 0} = \frac{b\theta_{y0}}{D} \qquad q_{\eta 1} = \frac{b\theta_{yb}}{D}$$

are the dimensionless rotational edge restraint parameters and $t_o^2 = ma^4/D$. Substituting $W(\xi,\eta,\tau) = U(\xi,\eta)g(\tau)$ into equation (A3) we obtain:

$$\frac{LU}{U} = -\frac{g_{\tau\tau}}{g}$$

Since the left side is a function only of ξ and η while the right side is a function of τ, they must both be equal to the same constant λ and the eigenvalue problem is:

$$LU - \lambda U = 0 \tag{A5}$$

$$\left.\begin{aligned} U_{\xi\xi} - q_{\xi 0}U_{\xi} &= 0 , \quad U = 0 \quad \text{on} \quad \xi = 0 \\ U_{\xi\xi} + q_{\xi 1}U_{\xi} &= 0 , \quad U = 0 \quad \text{on} \quad \xi = 1 \\ U_{\eta\eta} - q_{\eta 0}U_{\eta} &= 0 , \quad U = 0 \quad \text{on} \quad \eta = 0 \\ U_{\eta\eta} + q_{\eta 1}U_{\eta} &= 0 , \quad U = 0 \quad \text{on} \quad \eta = 1 \end{aligned}\right\} \tag{A6}$$

$$g_{\tau\tau} + \lambda g = 0 \tag{A7}$$

From equation (A7) the circular frequencies are given by $\omega_n = (1/t_o)\sqrt{\lambda_n}$. An approximate solution of the eigenvalue problem can be obtained by Galerkin's method as follows:

Assume a solution in the form:

$$U(\xi,\eta) = \sum_{j=1}^{J} C_j U_j(\xi,\eta)$$

where each U_j satisfies the boundary conditions.

Substituting in equation (A5) we obtain:

$$\sum_{j=1}^{J} (LU_j - \lambda U_j)C_j = 0 \tag{A8}$$

Now multiply by U_i and integrate over the panel to obtain:

$$\sum_{j=1}^{J} \int_0^1 \int_0^1 (U_i L U_j - \lambda U_i U_j) d\xi \, d\eta \, C_j = 0 , \qquad i = 1, 2, \ldots U \tag{A9}$$

or, in matrix form:

$$(A - \lambda B)C = 0 \tag{A10}$$

where

$$\left.\begin{aligned} a_{ij} &= \int_0^1 \int_0^1 U_i L U_j \, d\xi \, d\eta \\ b_{ij} &= \int_0^1 \int_0^1 U_i U_j \, d\xi \, d\eta \end{aligned}\right\} \tag{A11}$$

Let

$$\left.\begin{aligned} U_j(\xi,\eta) &= \Psi_m(\xi)\phi_n(\eta) \\ U_i(\xi,\eta) &= \Psi_r(\xi)\phi_s(\eta) \end{aligned}\right\} \tag{A12}$$

where

$$\left.\begin{aligned} \Psi_m(\xi) &= \sin(\alpha_\xi \xi + \beta_\xi)\sin m\pi\xi \\ \phi_n(\eta) &= \sin(\alpha_\eta \eta + \beta_\eta)\sin n\pi\eta \end{aligned}\right\} \tag{A13}$$

Ψ_m and ϕ_n satisfy the displacement boundary conditions and α_ξ, β_ξ, α_η, β_η are chosen to satisfy the remaining boundary conditions.

Substituting equations (A12) and (A13) into (A6) we find that α_ξ, β_ξ must satisfy the following equations:

$$2\alpha_\xi \cos \beta_\xi - q_{\xi 0} \sin \beta_\xi = 0 \tag{A14}$$

$$(2\alpha_\xi \cos \alpha_\xi + q_{\xi 1} \sin \alpha_\xi)\cos \beta_\xi + (q_{\xi 1} \cos \alpha_\xi - 2\alpha_\xi \sin \alpha_\xi)\sin \beta_\xi = 0 \tag{A15}$$

with corresponding equations for α_η, β_η.

Eliminating β results in:

$$(4\alpha_\xi^2 - q_{\xi 0}q_{\xi 1})\tan \alpha_\xi - 2\alpha_\xi(q_{\xi 0} + q_{\xi 1}) = 0 \qquad \text{(A16)}$$

Equation (A16) has one nontrivial root in the interval 0 to π (note that $\alpha_\xi = 0$ gives a function that satisfies simple support boundary conditions ($q_{\xi 0} = q_{\xi 1} = 0$), and $\alpha_\xi = \pi$ satisfies clamped conditions ($q_{\xi 0} = q_{\xi 1} = \infty$)), which may be calculated numerically for arbitrary values of $q_{\xi 0}$, $q_{\xi 1}$.

From equation (A14), $\tan \beta_\xi = 2\alpha_\xi/q_{\xi 0}$ which determines β_ξ once α_ξ is known.

Substituting equations (A12) into (A11) we have

$$a_{ij} = \int_0^1 \Psi_r \Psi_m^{iv}\, d\xi \int_0^1 \phi_s \phi_n\, d\eta + 2\frac{a^2}{b^2} \int_0^1 \Psi_r \Psi_m^{ii}\, d\xi \int_0^1 \phi_s \phi_n^{ii}\, d\eta$$

$$+ \frac{a^4}{b^4} \int_0^1 \Psi_r \Psi_m\, d\xi \int_0^1 \phi_s \phi_n^{iv}\, d\eta$$

$$b_{ij} = \int_0^1 \Psi_r \Psi_m\, d\xi \int_0^1 \phi_s \phi_n\, d\eta$$

The integrals are straightforward, resulting in

$$\int_0^1 \Psi_r \Psi_m\, d\xi = 2D_{rm} + \frac{1}{4}\delta_{rm}$$

$$\int_0^1 \Psi_r \Psi_m^{ii}\, d\xi = (2\alpha_\xi^2 - m^2\pi^2 - r^2\pi^2)D_{rm} - \frac{1}{4}(\alpha_\xi^2 + m^2\pi^2)\delta_{rm}$$

$$\int_0^1 \Psi_r \Psi_m^{iv}\, d\xi = 2\left[-3\alpha_\xi^4 + r^2m^2\pi^4 + \alpha_\xi^2(r^2 + m^2)\pi^2\right]D_{rm}$$

$$+ \frac{1}{8}\left[(\alpha_\xi + m\pi)^4 + (\alpha_\xi - m\pi)^4\right]\delta_{rm}$$

where

$$\delta_{rm} = \begin{cases} 0 & \text{if } r \neq m \\ 1 & \text{if } r = m \end{cases}$$

is the Kronecker delta and

$$D_{rm} = \frac{rm\pi^2\alpha_\xi\left[(-1)^{r+m}\sin 2(\alpha_\xi + \beta_\xi) - \sin 2\beta_\xi\right]}{16\left[\alpha_\xi + (r+m)\frac{\pi}{2}\right]\left[\alpha_\xi - (r+m)\frac{\pi}{2}\right]\left[\alpha_\xi + (r-m)\frac{\pi}{2}\right]\left[\alpha_\xi - (r-m)\frac{\pi}{2}\right]}$$

with corresponding integrals for ϕ_m. At

$$\alpha_\xi = \pm(r \pm m)\frac{\pi}{2}$$

D_{rm} contains removable singularities. If α_ξ is too close to a singularity, numerical accuracy will be impaired in evaluating D_{rm}; however, in that case the singularity may be removed analytically by expanding the numerator of D_{rm} in a Taylor series about $\pm (r \pm m)(\pi/2)$. The result will be:

$$D_{rm} = \frac{rm\pi^2\alpha_\xi \sum_{j=1}^{\infty} \frac{2^j}{j!}\sin\left(2\beta_\xi + \frac{j\pi}{2}\right)\left[\alpha_\xi \pm (r \pm m)\frac{\pi}{2}\right]^j}{16\left[\alpha_\xi + (r+m)\frac{\pi}{2}\right]\left[\alpha_\xi - (r+m)\frac{\pi}{2}\right]\left[\alpha_\xi + (r-m)\frac{\pi}{2}\right]\left[\alpha_\xi - (r-m)\frac{\pi}{2}\right]}$$

The matrix eigenvalue problem $(A - \lambda B)C = 0$ (eq. (A10)) can be placed in standard form in a numerically stable way utilizing a method given in reference 14. Factor B into the product TT^T of a lower triangular matrix T and its transpose T^T. Let $C = (T^T)^{-1}Y$ and we have $(A - \lambda TT^T)(T^T)^{-1}Y$. Multiply by T^{-1} to give $[T^{-1}A(T^T)^{-1} - \lambda I]Y = 0$ and the problem is in standard form.

NUMERICAL CALCULATIONS

Eigenvalues and eigenvectors have been calculated by programs available from SHARE, NUEIG 5, and GIVHO (refs. 15, 16). In the computations, 10 modes were used in the long direction of the panel and 5 modes in the short direction.

In figure 15 $\sqrt{\lambda_n}$ is plotted versus $q_\xi = q_{\xi 0} = q_{\xi 1}$ for $a/b = 0.5$ and $q_\eta = 2q_\xi$ to indicate the effect of varying the edge condition from simply

supported to clamped. Note that $q_\eta = 2q_\xi$ corresponds to the case of equal dimensional spring constants $\theta_x = \theta_y$ for $a/b = 0.5$.

The eigenvalues for perfectly clamped edges as shown in figure 15 were calculated by Galerkin's method using 14 clamped beam modes in both the spanwise and chordwise directions.

REFERENCES

1. Muhlstein, Lado, Jr.; Gaspers, Peter A., Jr.; and Riddle, Dennis W.: An Experimental Study of the Influence of the Turbulent Boundary Layer on Panel Flutter. NASA TN D-4486, 1968.

2. Dowell, E. H.; and Voss, H. M.: Experimental and Theoretical Panel Flutter Studies in the Mach Number Range of 1.0 to 5.0. ASD-TDR-63-449, The Boeing Co., Seattle, Washington, Dec. 1963. Also, Theoretical and Experimental Panel Flutter Studies in the Mach Number Range 1.0 to 5.0. AIAA J., vol. 3, no. 12, Dec. 1965, pp. 2292-2304.

3. Lock, M. H.; and Fung, Y. C.: Comparative Experimental and Theoretical Studies of the Flutter of Flat Panels in a Low Supersonic Flow. GALCIT 95 or AFOSR TN 670, Guggenheim Aero. Lab., Calif. Inst. Tech., Pasadena, Calif., May 1961.

4. Dixon, Sidney C.: Comparison of Panel Flutter Results From Approximate Aerodynamic Theory With Results From Exact Inviscid Theory and Experiment. NASA TN D-3649, 1966.

5. Spiegel, Joseph M.; and Lawrence, Leslie F.: A Description of the Ames 2- by 2-Foot Transonic Wind Tunnel and Preliminary Evaluation of Wall Interference. NACA RM A55I21, 1956.

6. Waller, Mary D.: A Simple Method of Finding Poisson's Ratio. Proc. Phys. Soc. (London), vol. 52, Sept. 1940, pp. 710-713.

7. Weeks, George E.; and Shideler, John L.: Effect of Edge Loadings on the Vibration of Rectangular Plates With Various Boundary Conditions. NASA TN D-2815, 1965.

8. Zeydel, Edmond F. E.: Large Deflection Panel Flutter. AFOSR Tech. Note 1952, Jan. 1962.

9. Zeydel, E. F. E.; and Kobett, D. R.: Flutter of Flat Plates With Partially Clamped Edges in the Low Supersonic Region. AIAA J., vol. 3, no. 1, Jan. 1965, pp. 17-22.

10. Cunningham, Herbert J.: Flutter Analysis of Flat Rectangular Panels Based on Three-Dimensional Supersonic Unsteady Potential Flow. NASA TR R-256, 1967.

11. Ketter, D. J.: Flutter of Flat, Rectangular, Orthotropic Panels. AIAA J., vol. 5, no. 1, Jan. 1967, pp. 116-124.

12. Zener, C.: Elasticity and Anelasticity of Metals. Univ. of Chicago Press, 1948.

13. Dowell, E. H.: Theoretical-Experimental Correlation of Plate Flutter Boundaries at Low Supersonic Speeds. AIAA J., vol. 6, no. 9, Sept. 1968, pp. 1810-1811.

14. Wilkinson, J. H.: The Algebraic Eigenvalue Problem. Clarendon Press, Oxford, 1965, p. 337.

15. Parlett, B. N.: NUEIG5 Eigenvalues of Real Matrices. SHARE Program, SDA 309801, 1964.

16. Ortega, J. M.: GIVHO Eigenvalues and Eigenvectors of Real Symmetric Matrices. SHARE Program, SDA 160A, 1965.

TABLE 1.- PANEL NATURAL FREQUENCIES, LOCATIONS OF NODE LINES,

EDGE CONDITIONS, AND MATERIAL CONSTANTS

(a) Invar panel

Location of node lines	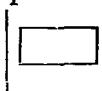			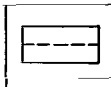	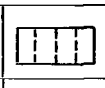
Measured natural frequencies, Hz	38.0	52.0	79.0	106.0	116.0
Theoretical natural frequencies for edge restraints, $q_\xi = 14$, $q_\eta = 110.0$, Hz	38.9	53.1	77.9	102.9	112.9
Deviation of measured frequencies from theoretical values, percent	-2.3	-2.1	1.4	3.0	2.8
Theoretical natural frequencies for clamped edges, $q_\xi = q_\eta = \infty$, Hz	46.4	60.1	84.4	120.9	119.6
Deviation of measured frequencies from theoretical values, percent	18.1	13.5	6.4	12.3	3.0

Panel characteristics

Panel dimensions:	9.00×18.00×0.0192 in.	
Edge conditions:	$q_x = 14$, $q_y = 110.0$	
Material:	Invar, 64 percent Fe, 36 percent Ni	
E:	21.0×10^6 lb/in.^{2}	Handbook
ν:	0.29	
ρ_s:	507.9 lb/ft^3	
α:	0.7×10^{-6} in./in./°F	

(b) Magnesium panel

Location of node lines		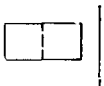		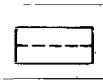	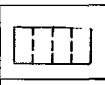
Measured natural frequencies, Hz	110.0	143.0	212.0	287.0	298.0
Theoretical natural frequencies for edge restraints, $q_\xi = 62$, $q_\eta = \infty$, Hz	110.1	144.9	207.0	287.7	295.5
Deviation of measured frequencies from theoretical values, percent	-.1	-1.3	2.4	-.2	.9
Theoretical natural frequencies for clamped edges, $q_\xi = q_\eta = \infty$, Hz	115.7	149.8	210.3	301.2	297.9
Deviation of measured frequencies from theoretical values, percent	-4.9	-4.5	.8	-4.7	.03

Panel characteristics

Panel dimensions:	9.00×18.00×0.0401 in.	
Edge conditions:	$q_x = 62$, $q_y = \infty$	
Material:	Magnesium alloy AZ 31B-H24	
E:	6.2×10^6 lb/in.^{2}	Measured, see p. 3
ν:	0.35	
ρ_s:	110.0 lb/ft^3	
α:	14.2×10^{-6} in./in./°F	

TABLE 2.- TABULATED PANEL FLUTTER DATA INVAR PANEL

Mach number	Wall displacement	Free-stream temperature	Dynamic pressure for multiples of subflutter response, psf					Boundary-layer thickness, in.				Flutter frequency, Hz	Reduced flutter frequency	Supersonic reduced flutter frequency	Mass ratio parameter	Cavity density ratio	Modified stiffness parameter	Stiffness parameter
M_∞	H, in.	T_∞, °R	q_{2x}	q_{3x}	q_{4x}	q_{5x}	$q_{6x}=q_F$	δ	$\delta_{m=1.0}$	δ^*	θ	f_F	k	K	μ	μ_c	k* (1)	k (2)
1.20	0	416.4	370	382	392	400	403	1.14	0.52	0.228	0.110	37	0.145	0.396	0.0166	0.0133	0.0309	0.0252
1.20	.30	412.5	273	304	315	321	325	.82	.32	.162	.076	42	.166	.452	.0135	.0107	.0310	.0253
1.20	.50	415.2	243	251	254	255	256	.66	.26	.134	.058	45	.177	.483	.0106	.0084	.0309	.0252
1.20	.80	411.4	208	215	217	219	221	.46	.25	.108	.045	46	.182	.496	.0092	.0073	.0311	.0254
1.30	0	396.8	423	443	451	458	464	1.15	.54	.262	.112	47	.175	.329	.0171	.0131	.0316	.0258
1.30	.80	397.0	267	275	277	279	280	.38	.16	.102	.038	52	.193	.364	.0103	.0078	.0316	.0258
1.30	1.00	396.6	261	263	264	265	265	.32	.14	.088	.038	53	.197	.371	.0098	.0074	.0316	.0258
1.40	.60	381.3	373	388	390	390	390	.47	.12	.105	.042	48	.169	.246	.0129	.0095	.0323	.0263
1.40	.80	381.0	349	366	370	370	370	.34	.12	.094	.033	52	.183	.267	.0123	.0090	.0323	.0263

[1]E = 21.0×10^6 lb/in.^{2} (Handbook).

[2]E = 14.1×10^6 lb/in.^{2} (See p. 8).

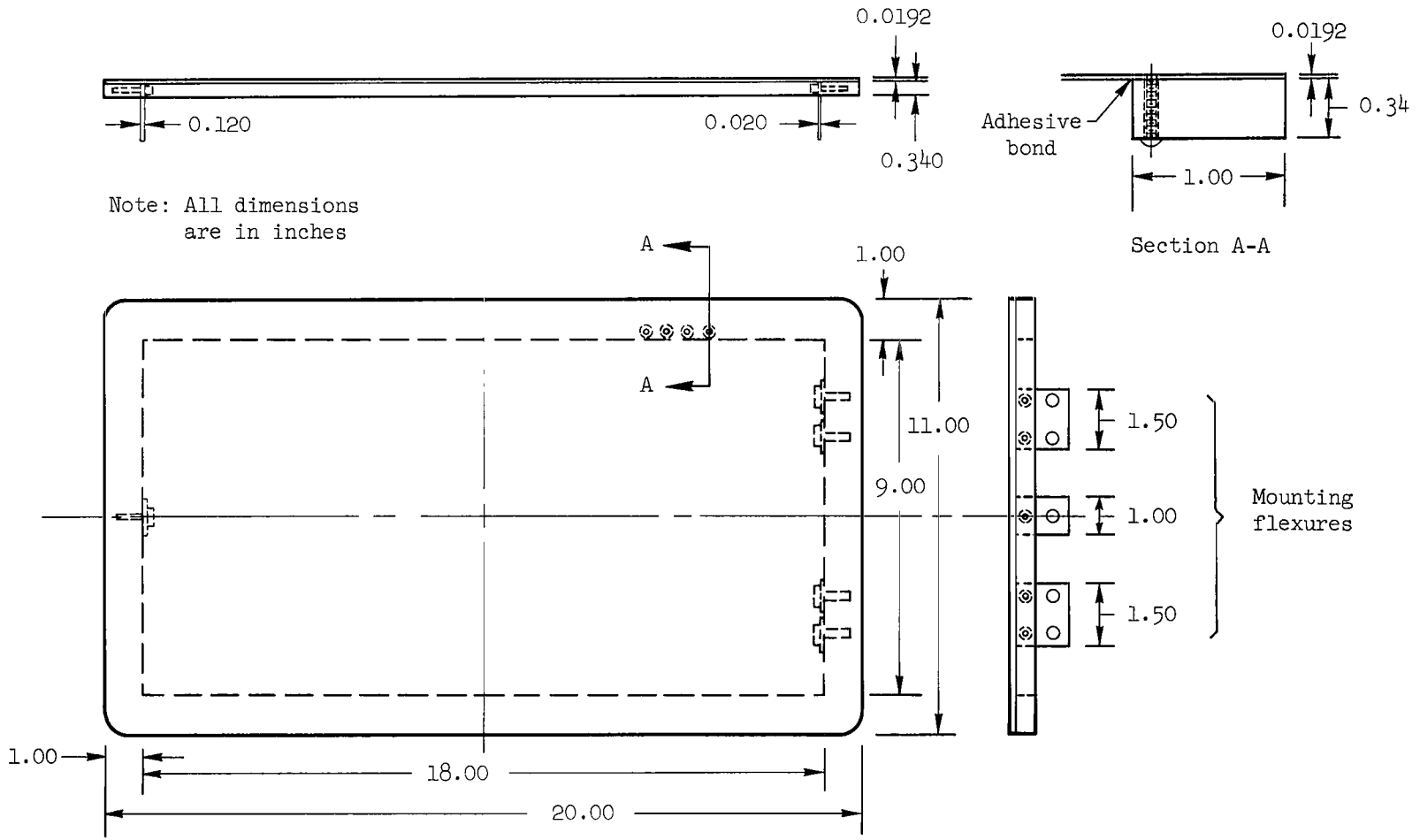

Figure 1.- Invar panel dimensions and construction details.

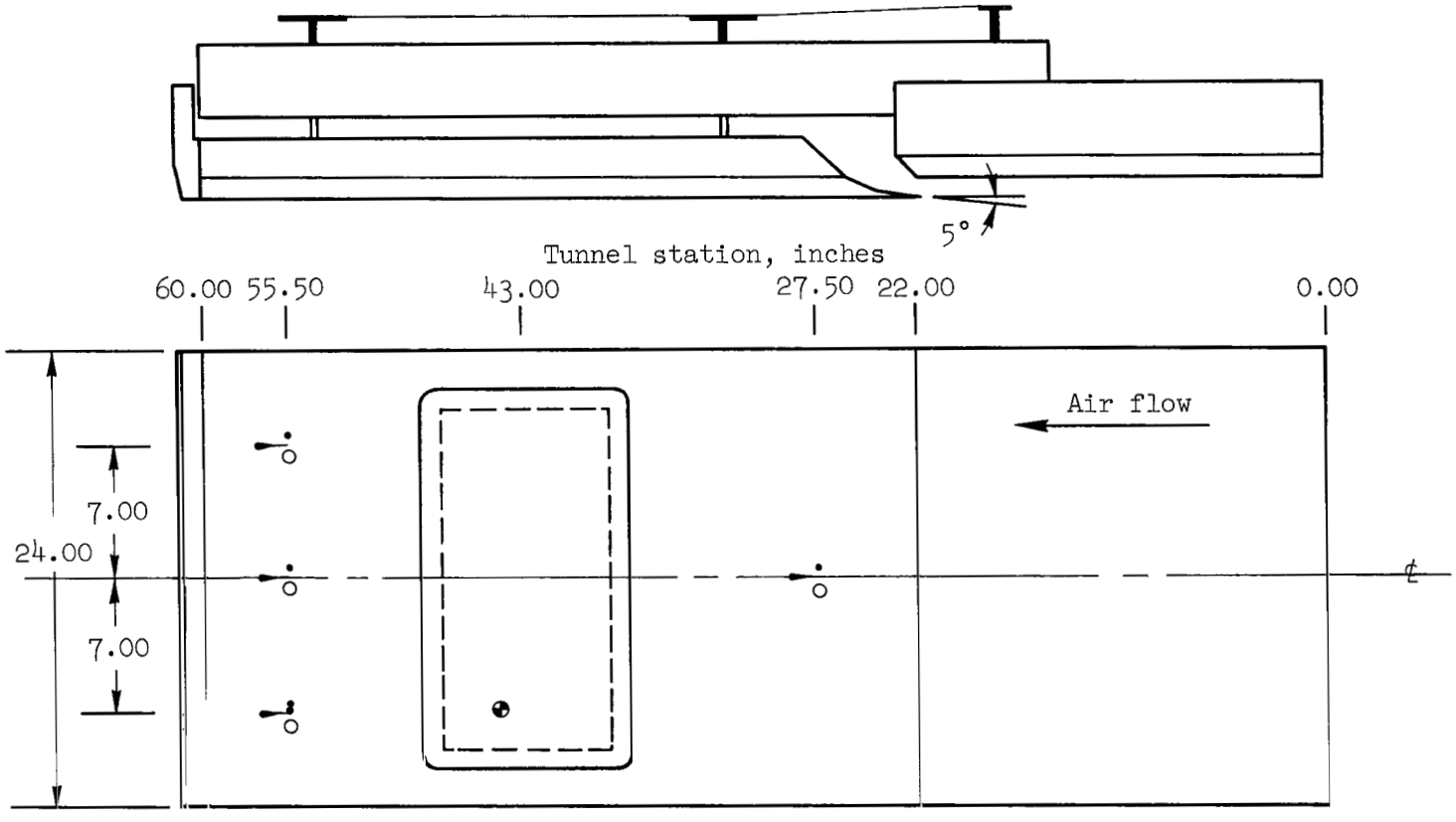

Figure 2.- Layout of variable boundary-layer test fixture.

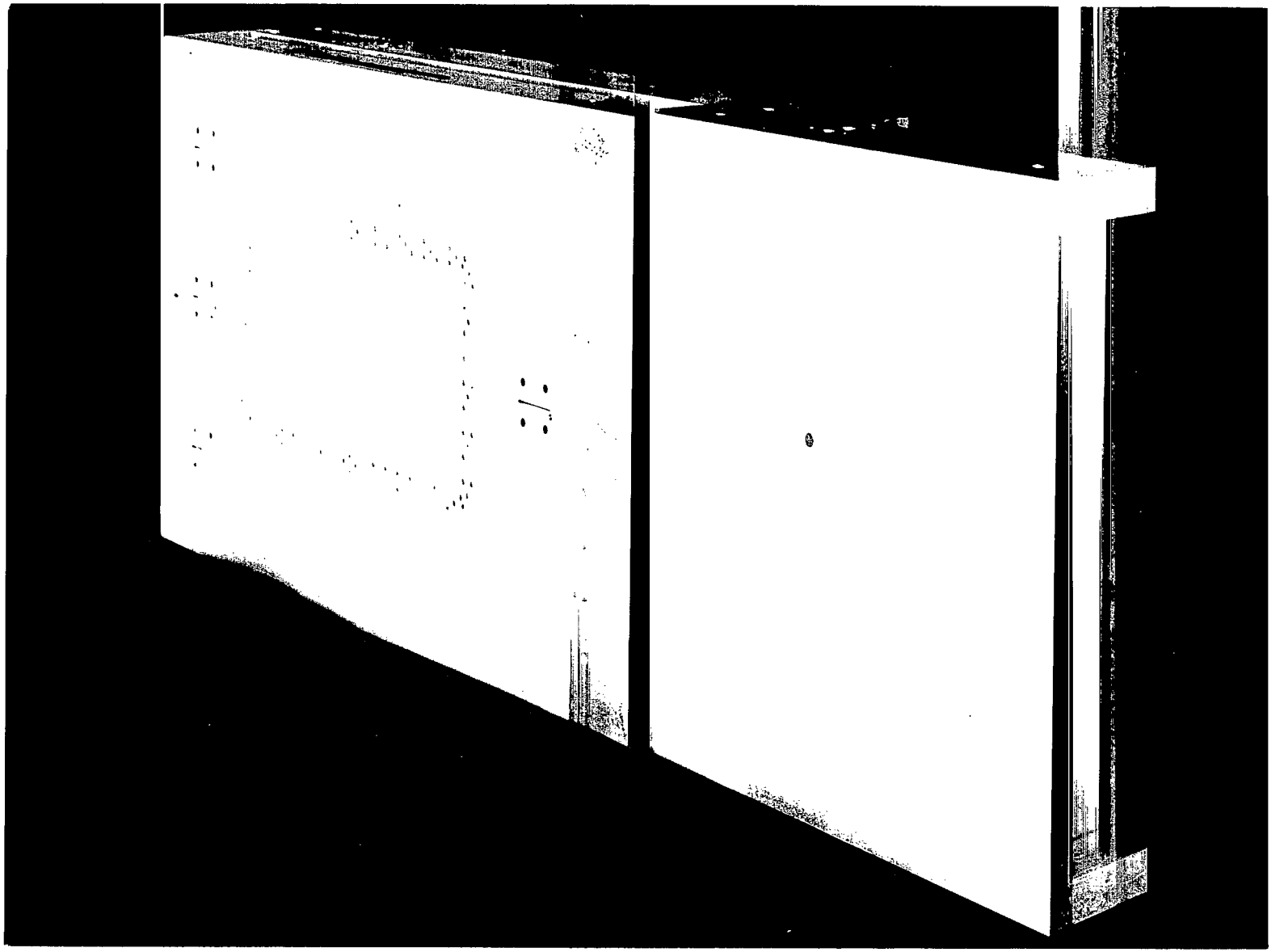

(a) Three-fourths front view of airstream side

A-39842

Figure 3.- Variable boundary-layer test fixture.

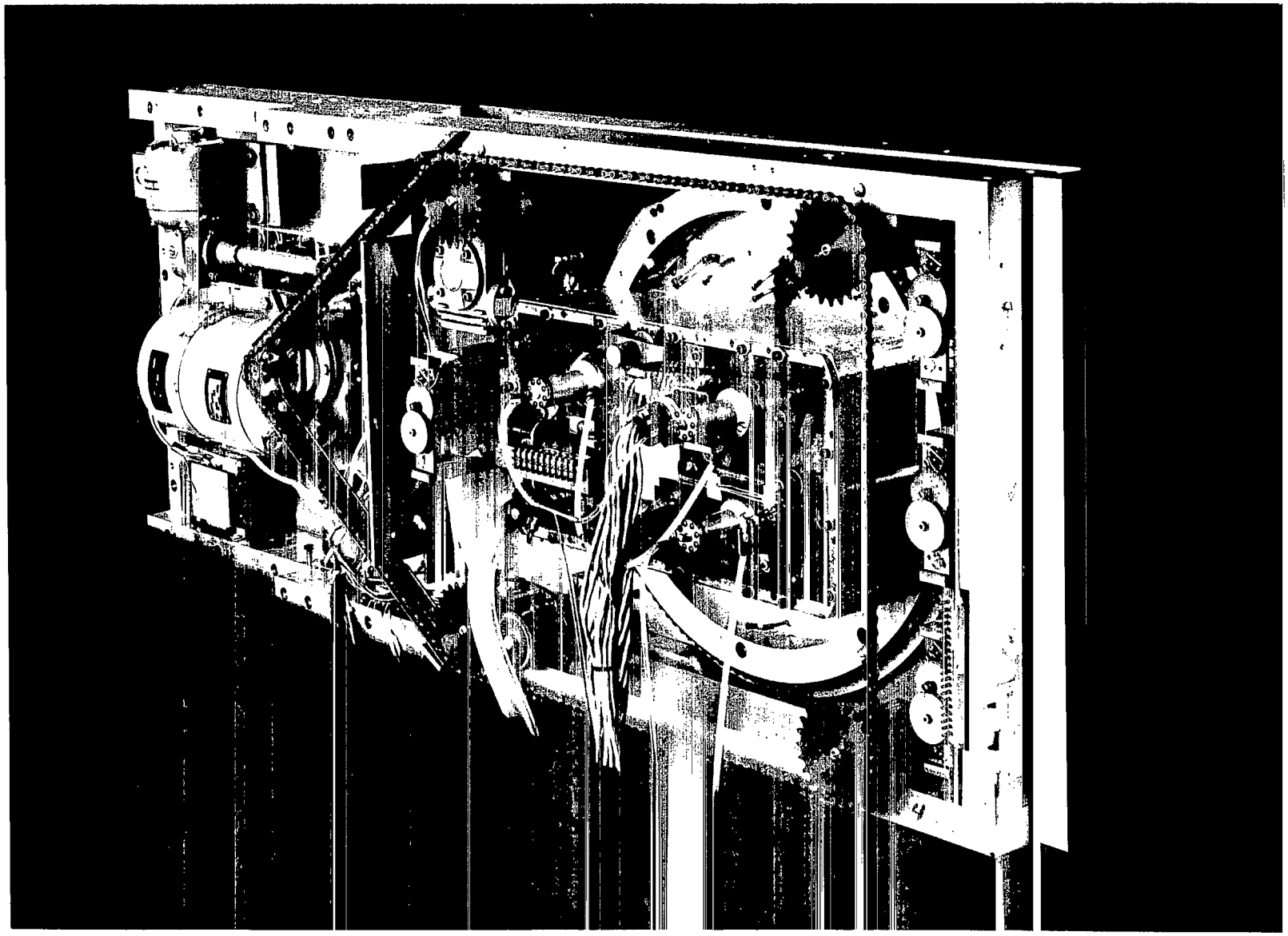

(b) Three-fourths rear view of plenum chamber side

A-39841

Figure 3.- Concluded.

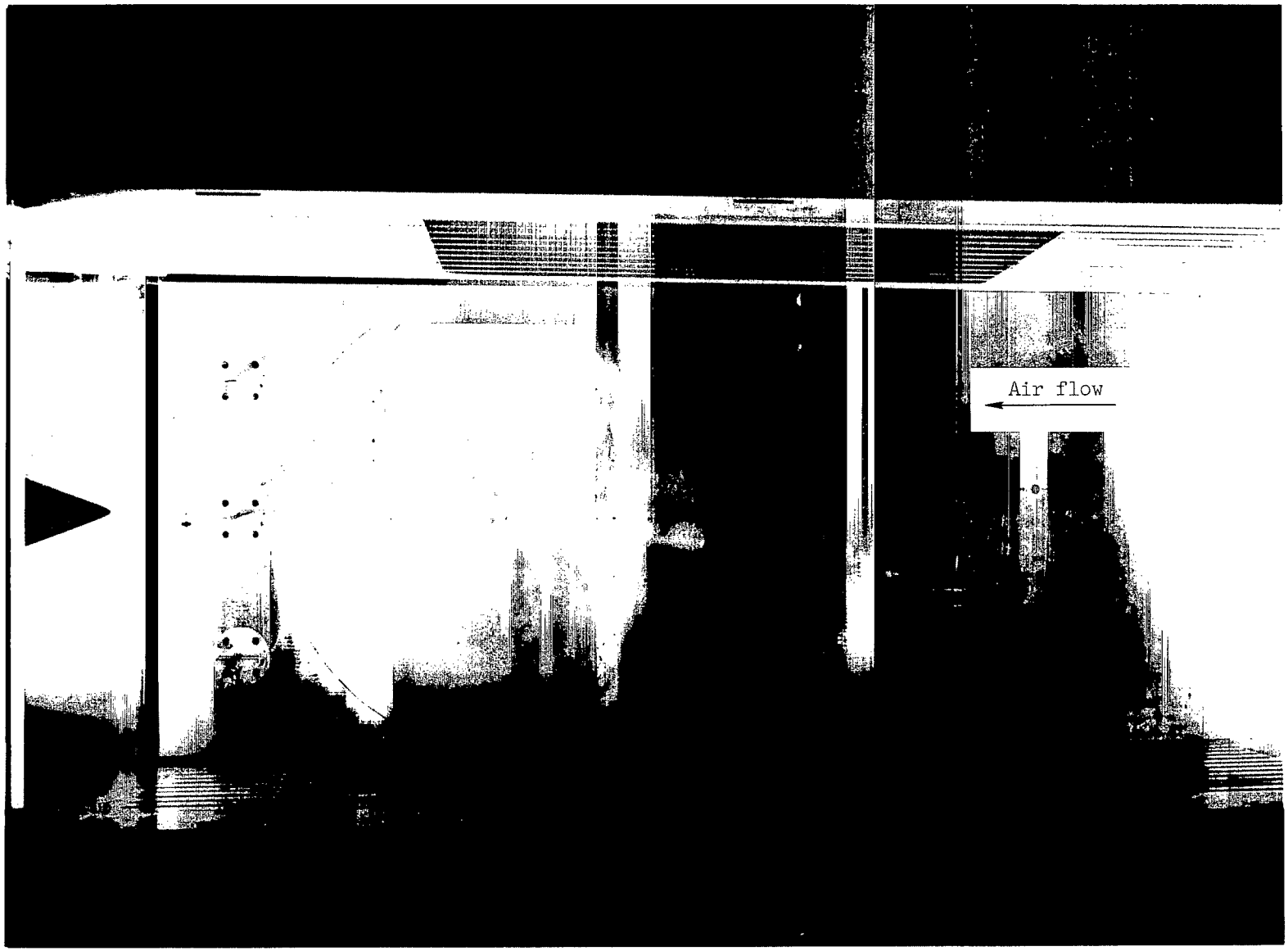

A-35851.1

Figure 4.- Panel with variable boundary-layer fixture installed in the 2-by 2-foot transonic wind tunnel.

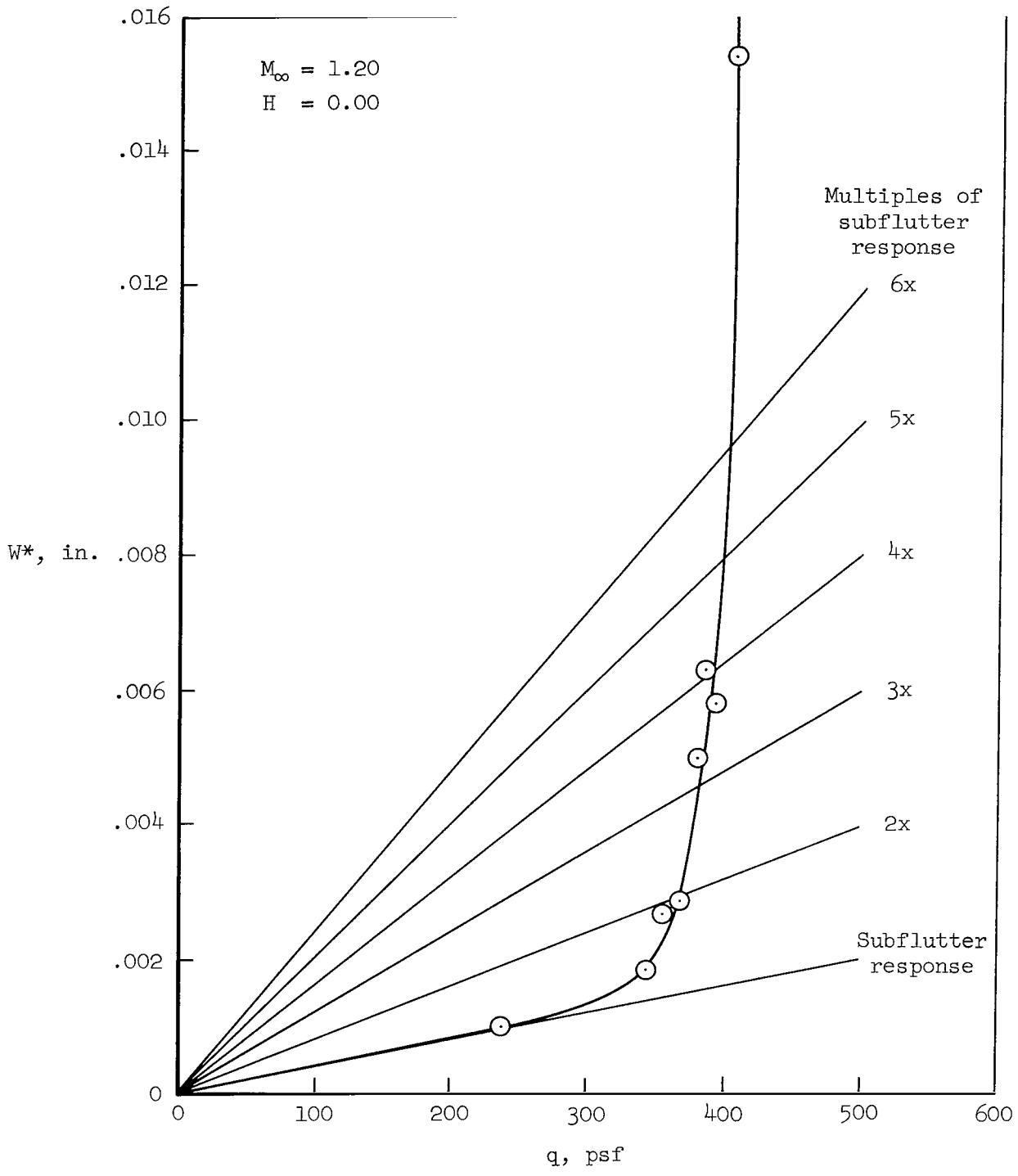

Figure 5.- Typical variation of maximum panel response with dynamic pressure.

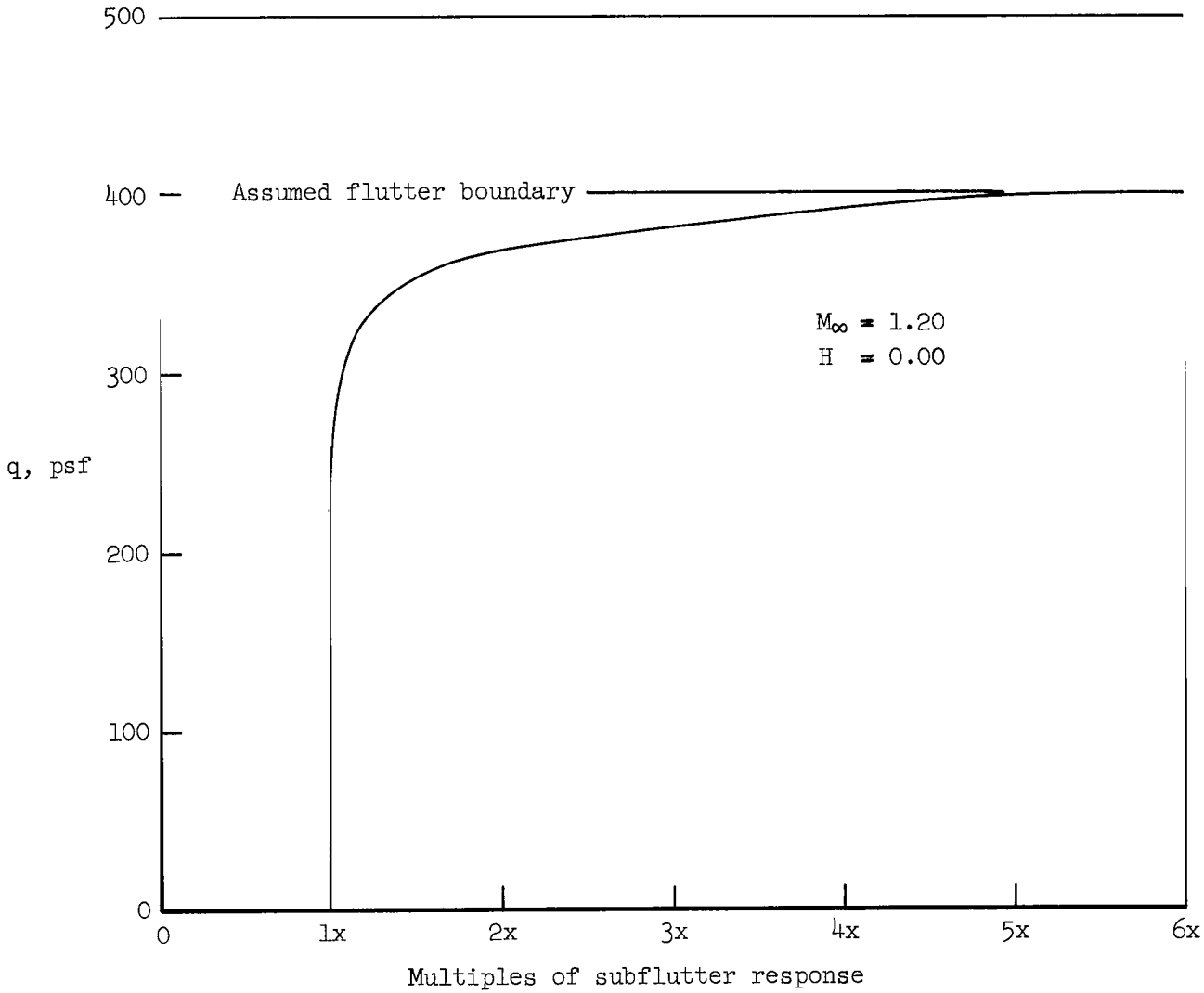

Figure 6.- Typical convergence of multiples of subflutter response with dynamic pressure.

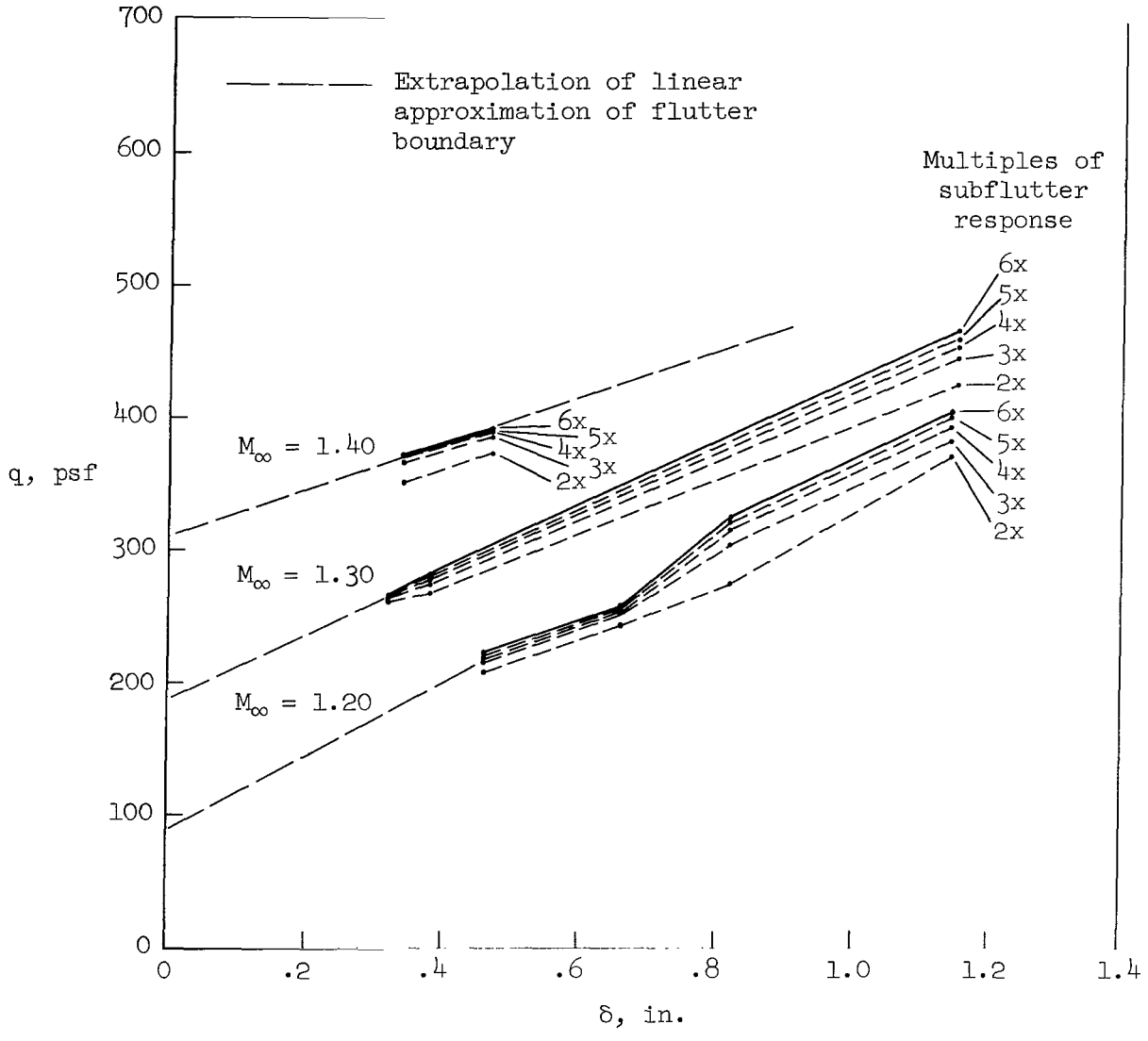

Figure 7.- Dynamic pressure for multiples of subflutter response as a function of boundary-layer thickness.

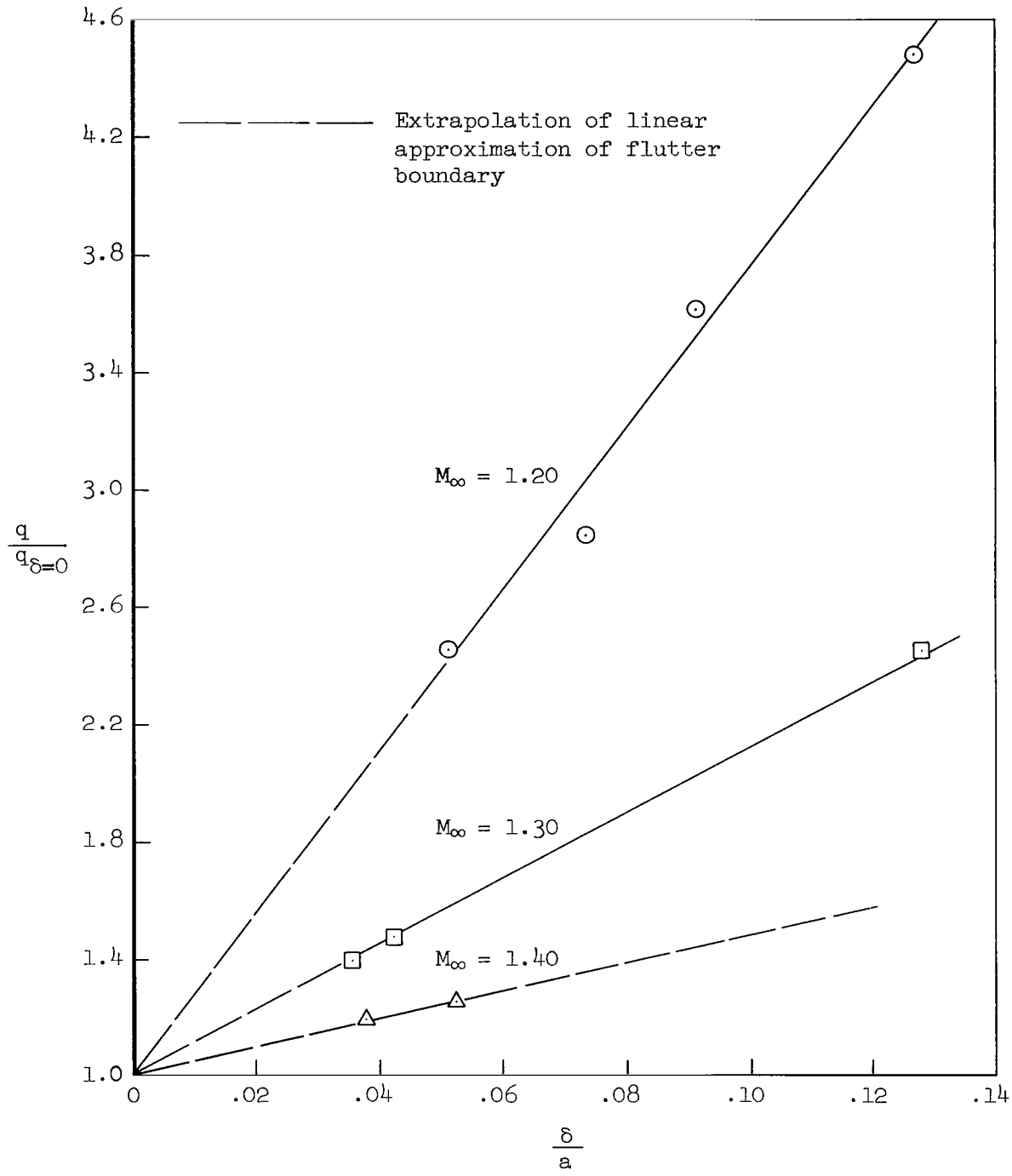

Figure 8.- Normalized flutter dynamic pressure as a function of normalized boundary-layer thickness.

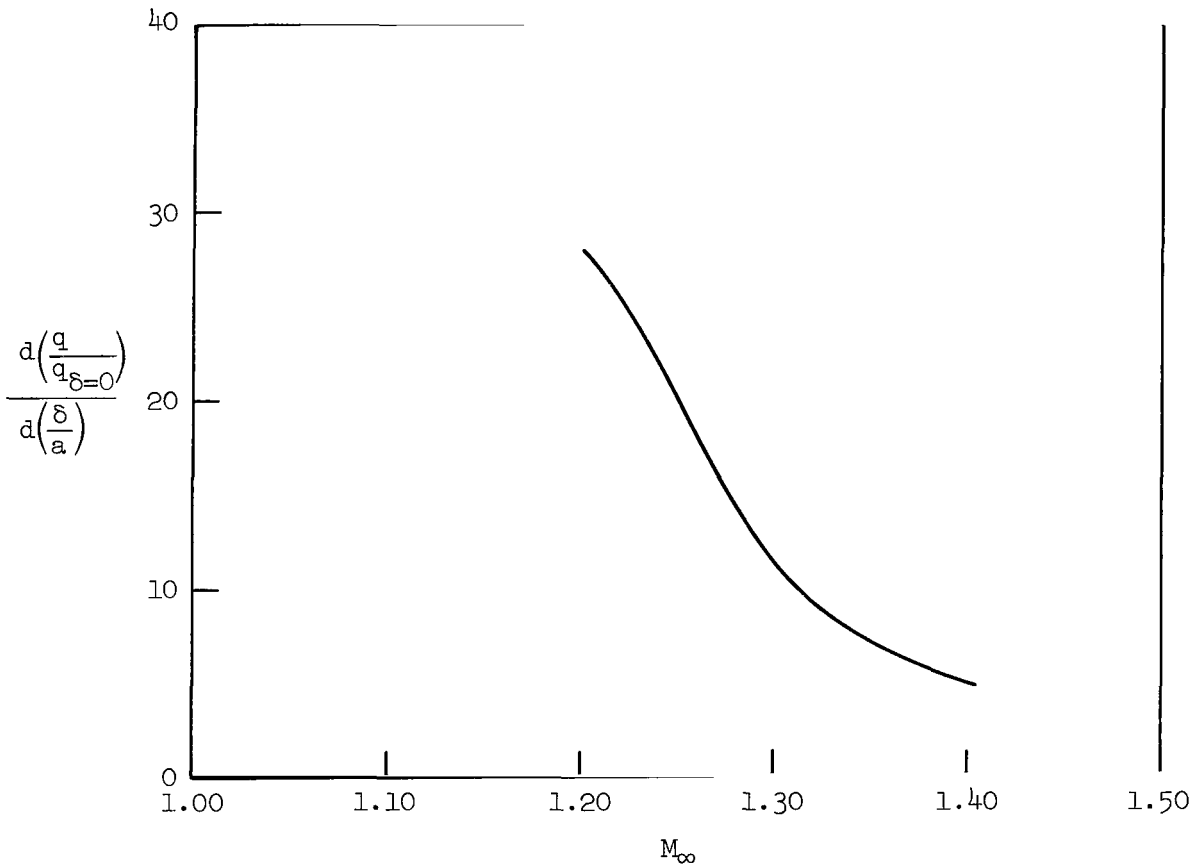

Figure 9.- Rate of change of normalized flutter dynamic pressure with respect to normalized boundary-layer thickness as a function of Mach number.

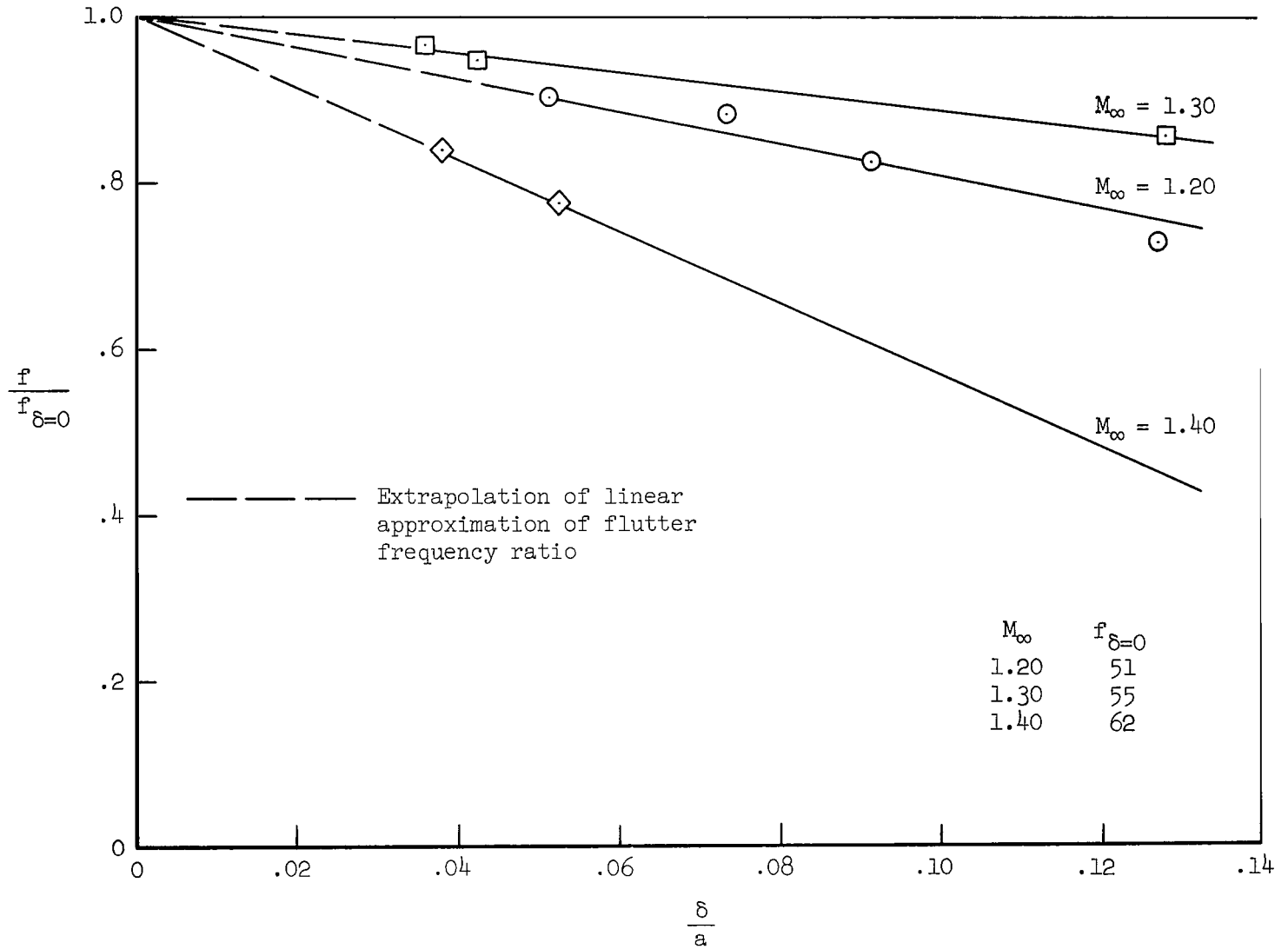

Figure 10.- Normalized flutter frequency as a function of the normalized boundary-layer thickness.

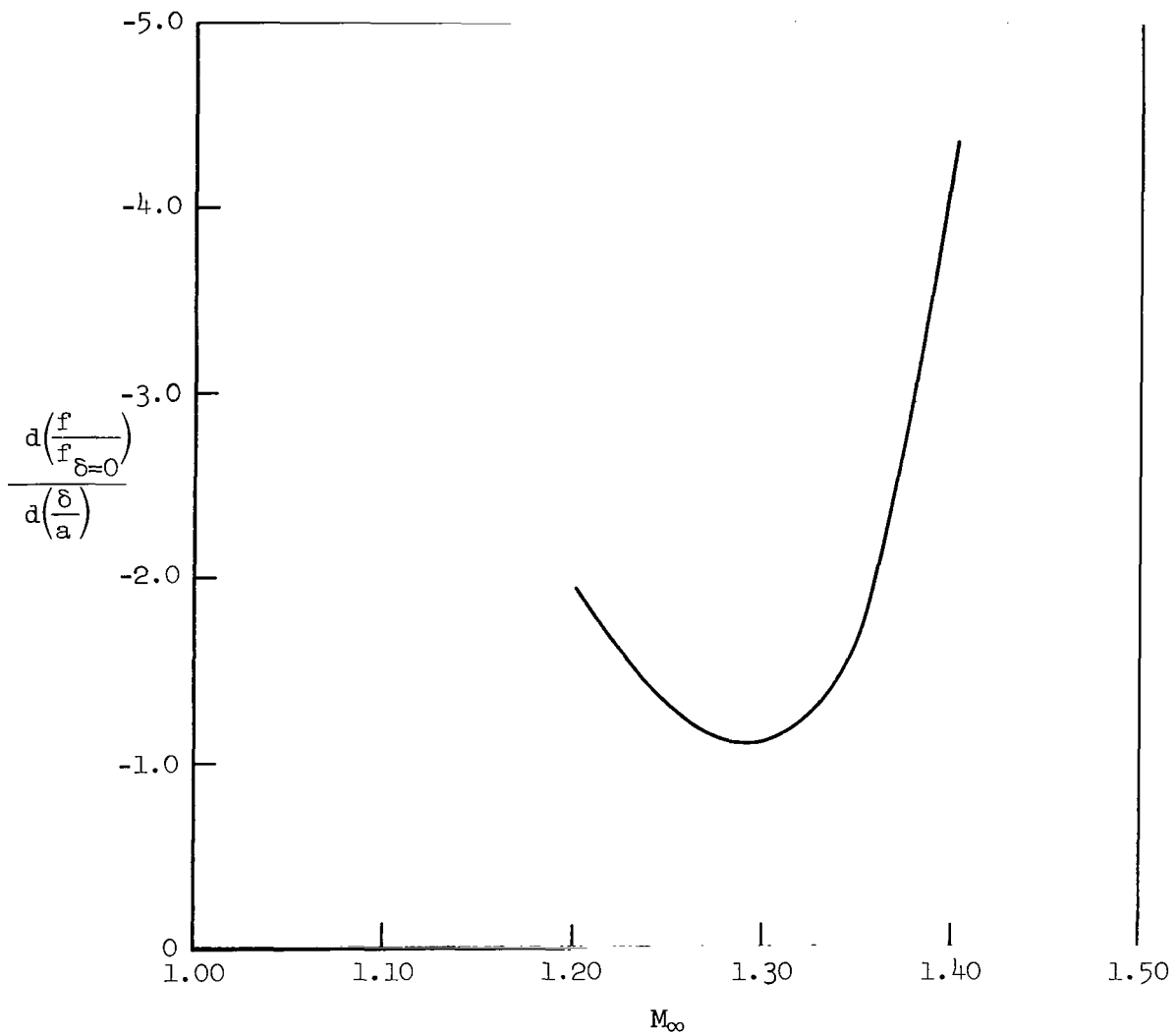

Figure 11.- Rate of change of normalized flutter frequency with respect to normalized boundary-layer thickness as a function of Mach number.

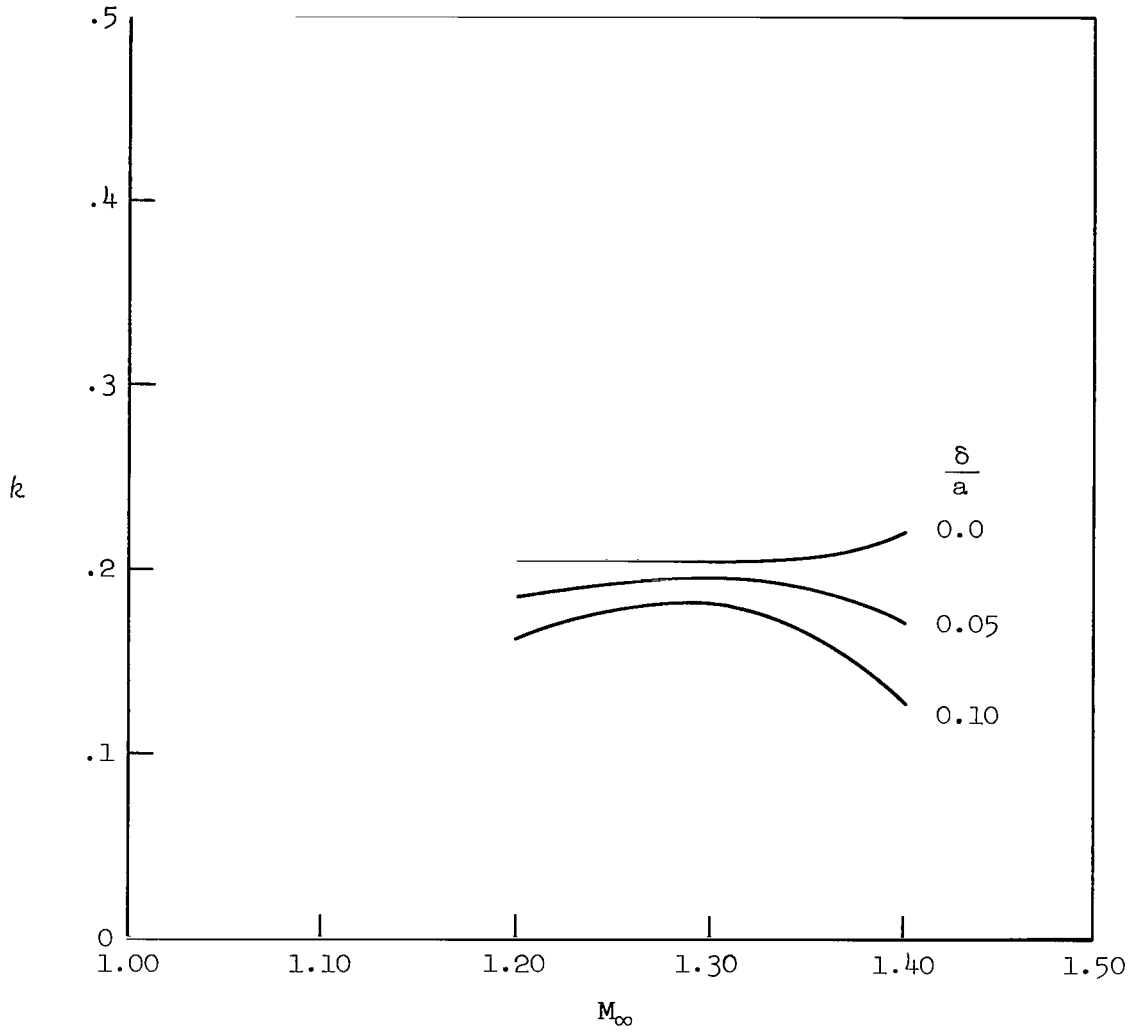

Figure 12.- Reduced frequency of flutter as a function of Mach number.

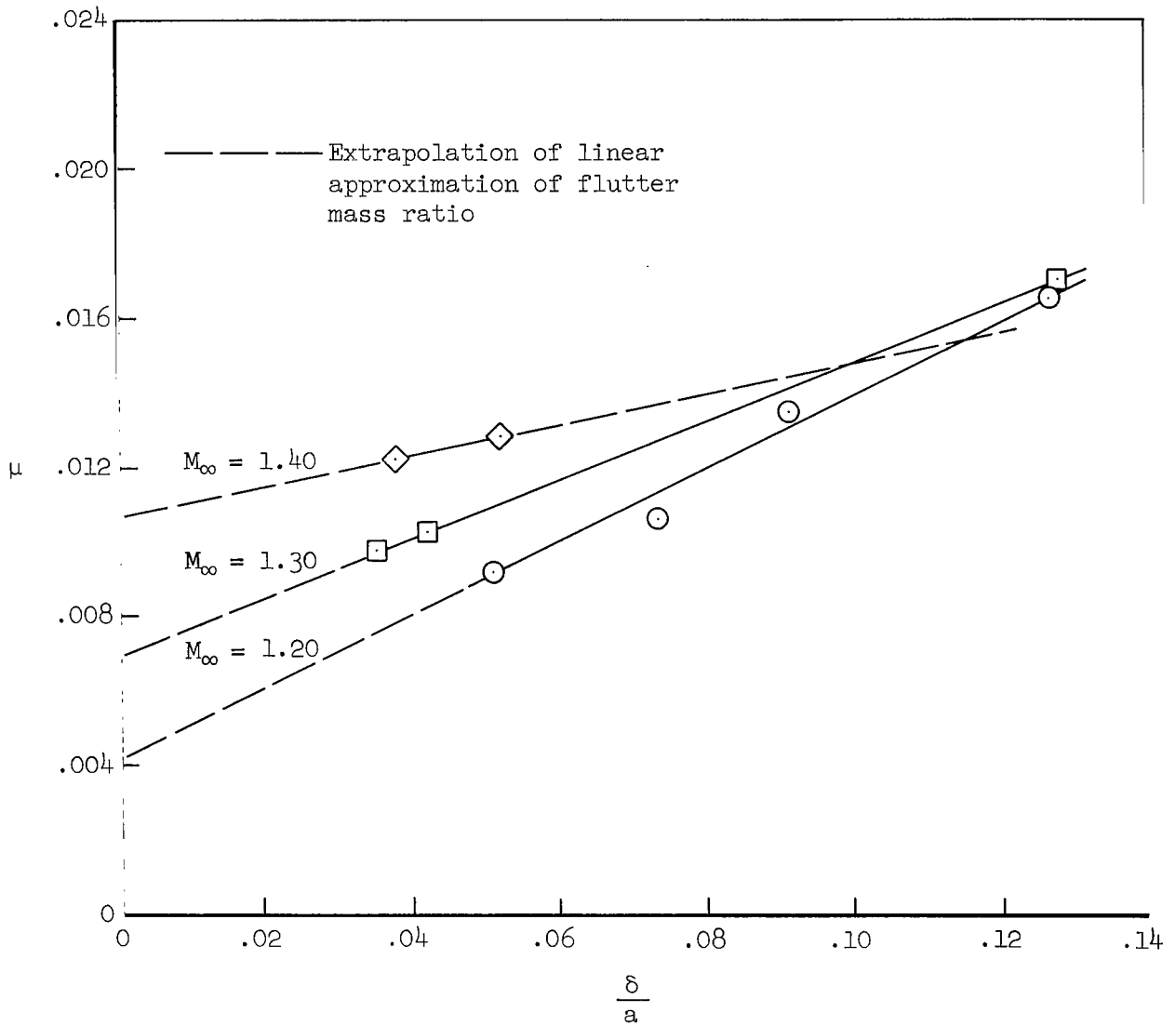

Figure 13.- Flutter mass ratio parameter as a function of the normalized boundary-layer thickness.

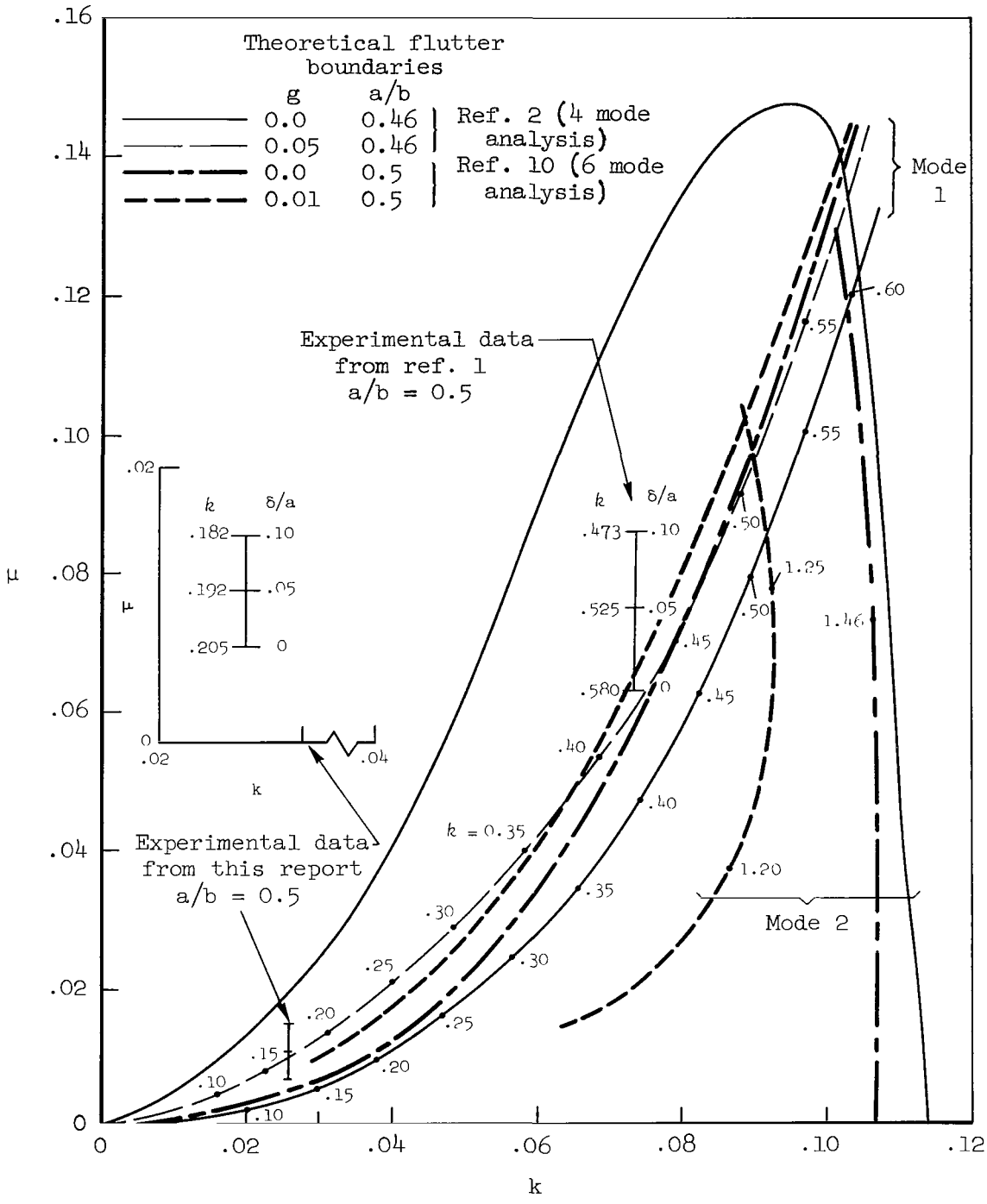

(a) Comparison at $M_\infty = 1.30$

Figure 14.- Comparison of experimental flutter points with theoretical stability boundaries in the stiffness parameter-mass ratio (k, μ) plane.

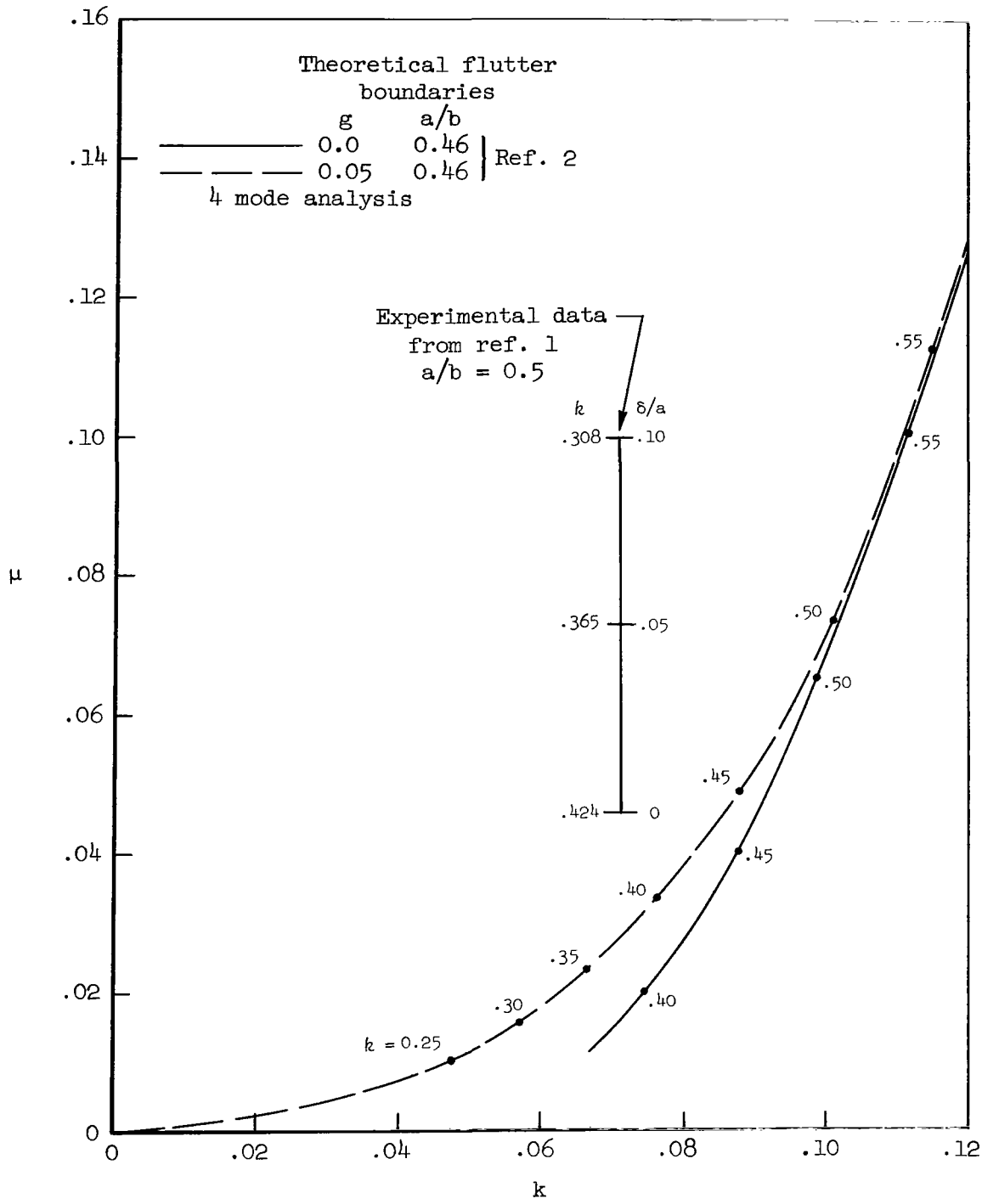

(b) Comparison at $M_\infty = 1.10$

Figure 14.- Continued.

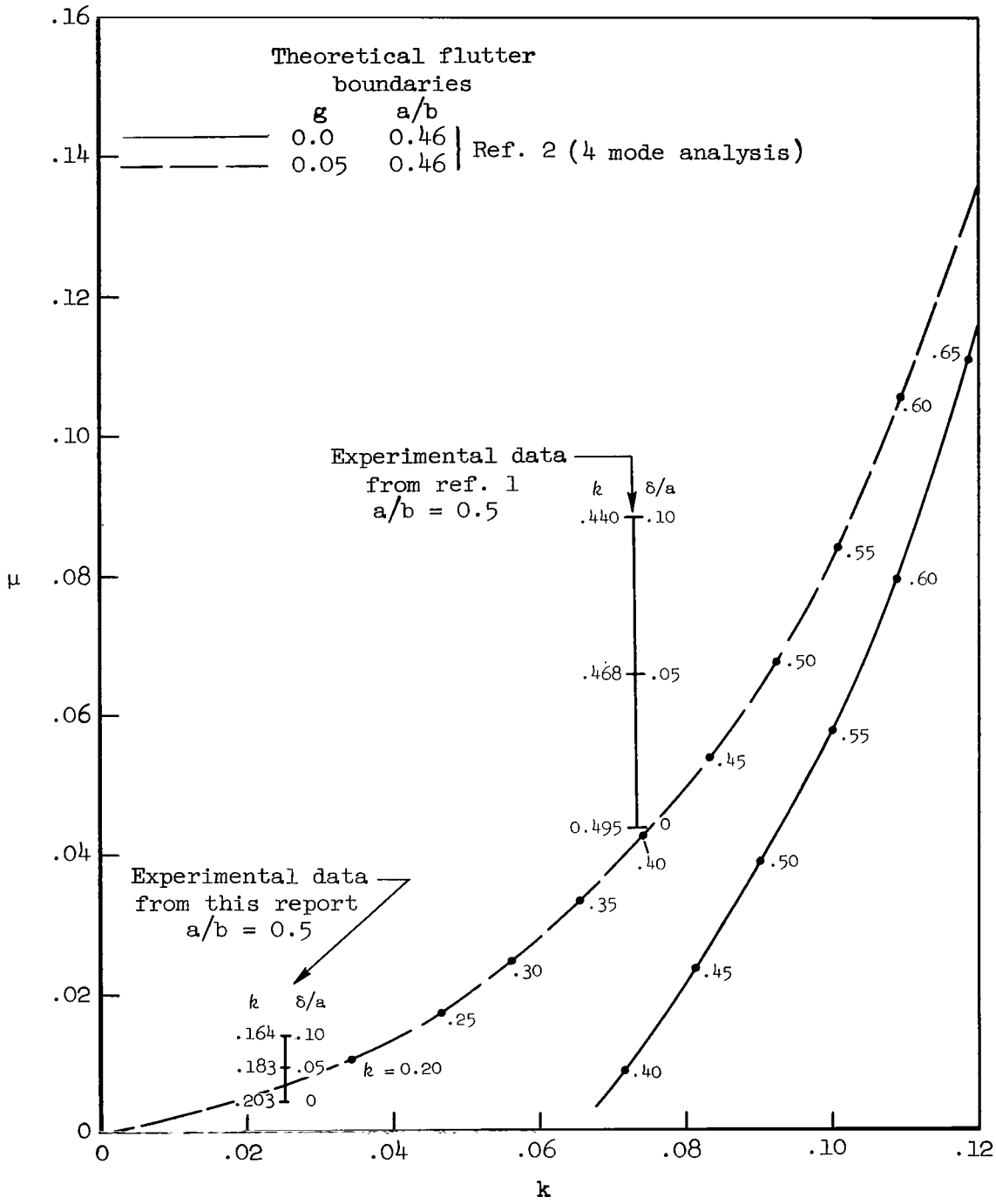

(c) Comparison at $M_\infty = 1.20$

Figure 14.- Continued.

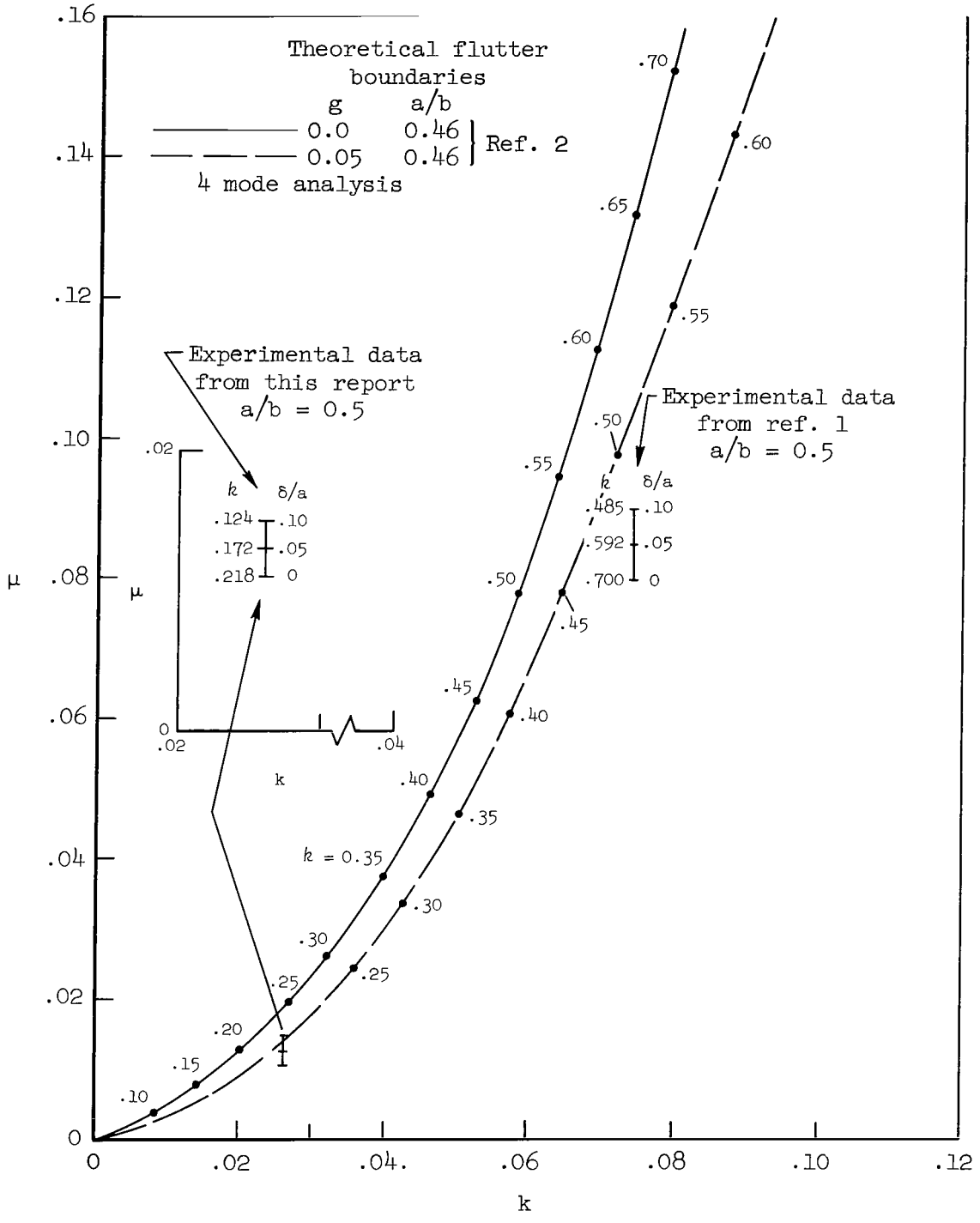

(d) Comparison at $M_\infty = 1.40$

Figure 14.- Concluded.

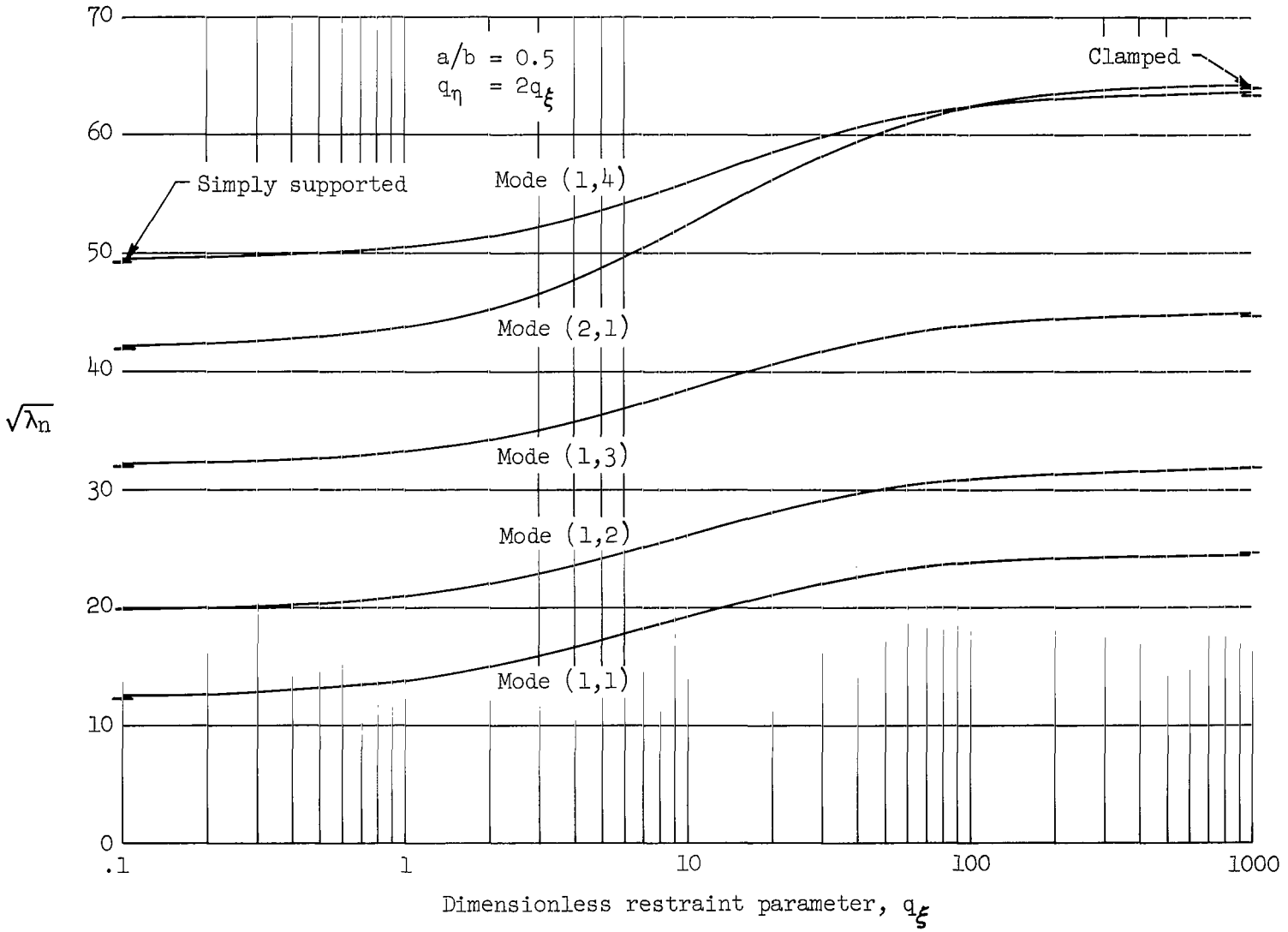

Figure 15.- Effect of rotational edge restraint on the eigenvalues of a rectangular plate.

NATIONAL AERONAUTICS AND SPACE ADMINISTRATION
WASHINGTON, D. C. 20546
OFFICIAL BUSINESS

FIRST CLASS MAIL

POSTAGE AND FEES PAID
NATIONAL AERONAUTICS AN
SPACE ADMINISTRATION

POSTMASTER: If Undeliverable (Section 158 Postal Manual) Do Not Retur

"The aeronautical and space activities of the United States shall be conducted so as to contribute . . . to the expansion of human knowledge of phenomena in the atmosphere and space. The Administration shall provide for the widest practicable and appropriate dissemination of information concerning its activities and the results thereof."

—NATIONAL AERONAUTICS AND SPACE ACT OF 1958

NASA SCIENTIFIC AND TECHNICAL PUBLICATIONS

TECHNICAL REPORTS: Scientific and technical information considered important, complete, and a lasting contribution to existing knowledge.

TECHNICAL NOTES: Information less broad in scope but nevertheless of importance as a contribution to existing knowledge.

TECHNICAL MEMORANDUMS: Information receiving limited distribution because of preliminary data, security classification, or other reasons.

CONTRACTOR REPORTS: Scientific and technical information generated under a NASA contract or grant and considered an important contribution to existing knowledge.

TECHNICAL TRANSLATIONS: Information published in a foreign language considered to merit NASA distribution in English.

SPECIAL PUBLICATIONS: Information derived from or of value to NASA activities. Publications include conference proceedings, monographs, data compilations, handbooks, sourcebooks, and special bibliographies.

TECHNOLOGY UTILIZATION PUBLICATIONS: Information on technology used by NASA that may be of particular interest in commercial and other non-aerospace applications. Publications include Tech Briefs, Technology Utilization Reports and Notes, and Technology Surveys.

Details on the availability of these publications may be obtained from:

SCIENTIFIC AND TECHNICAL INFORMATION DIVISION

NATIONAL AERONAUTICS AND SPACE ADMINISTRATION

Washington, D.C. 20546